Chemical Engineering & Processing: Process Intensification 174 (2022) 108862

Contents lists available at ScienceDirect

Chemical Engineering and Processing - Process Intensification

journal homepage: www.elsevier.com/locate/cep

Experimental and numerical study on thermodynamic characteristics of a vacuum membrane distillation system based on mechanical vapor recompression for sulfuric acid waste

Zetian Si [a], Dong Han [b], Yulei Xing [c], Jiawei Xiang [a,*]

[a] College of Mechanical and Electrical Engineering, Wenzhou University, Wenzhou 325035, Zhejiang, China
[b] College of Energy and Power Engineering, Nanjing University of Aeronautics and Astronautics, Nanjing 210016, Jiangsu, China
[c] The Institute of Seawater Desalination and Multipurpose Utilization, Ministry of Natural Resources (MNR), Tianjin 300192, China

ARTICLE INFO

Keywords:
Sulfuric acid waste
Vacuum membrane distillation
Mechanical vapor recompression
Separation efficiency
Performance coefficient
Exergy

ABSTRACT

Energy conservation and emission reduction in the field of industrial wastewater treatment have attracted worldwide attention. This study focused on the concentration and recovery of industrial sulfuric acid waste by a vacuum membrane distillation system based on mechanical vapor recompression (VMD-MVR). Mathematical models were built considering the mass and energy conservation principles and relevant thermal equilibrium theory, and an experimental platform, which was suitable for sulfuric acid solution, with excellent corrosion resistance was also constructed. Initially, the performance of VMD-MVR from the energetic and exergetic standpoints was evaluated based on the experimental data. Furthermore, the effects of critical parameters on compression and condensation heat transfer in VMD-MVR were simulated and revealed, and exergy destruction analysis was conducted using various selected parameters. The obtained experimental results indicated that VMD-MVR exhibited a membrane flux of 1.7 $kg{\cdot}m^{-2}{\cdot}h^{-1}$, separation efficiency of 99.9%, and performance coefficient (*COP*) of 7.88 under the following conditions: feed concentration: 5%; feed temperature: 353.0 K; feed velocity: 1.6 $m{\cdot}s^{-1}$; permeate side pressure: 45 kPa; heat transfer temperature difference (ΔT_{hex}): 2 K; and compressor frequency: 40 Hz. The exergy input, exergy destruction, exergy output, and exergy efficiency were 4.95 kW, 4.691 kW, 0.259 kW, and 5.24%, respectively. Moreover, according to the numerical simulation results, with a decrease in the feed concentration and ΔT_{hex} or with an increase in the feed temperature, feed velocity, and permeate side pressure, the compression ratio and exergy destruction in VMD-MVR decreased, whereas the *COP* increased.

1. Introduction

Along with the science and technology progress and rapid social economy development, sulfuric acid, which is a basic hazardous chemical, is being applied in various fields including steel, petrochemical, chlor-alkali, pharmaceutical, papermaking, and military projects. However, in these fields, a tremendous amount of sulfuric acid solution is inevitably generated as a by-product owing to inadequate production equipment, backward technical conditions, and weak awareness of environmental protection. The discharge of this sulfuric acid waste without pretreatment not only leads to resource wastage, but also poses a considerable potential threat to safety and the environment. Therefore, promoting and improving the comprehensive utilization of sulfuric acid waste is highly important [1–3].

Several sulfuric acid waste treatment methods, such as neutralization reaction, high temperature pyrogenation, extraction, oxidative decomposition, single effect evaporation, multistage flash evaporation, have been proposed and gradually developed worldwide. However, the application of the abovementioned methods is limited by numerous problems including low separation efficiency, high energy consumption, poor operation stability, serious secondary pollution, and complicated configuration. Recently, a very promising method called membrane distillation (MD), based on thermal distillation and membrane separation, has been proposed, and various studies have been reported on it. Due to the advantages of excellent separation performance and low operation temperature and pressure, MD has been applied in many areas including desalination, wastewater treatment, food processing, and pharmaceuticals [4,5]. In MD, a hydrophobic microporous membrane is utilized as a physical support to achieve the separation of water

* Corresponding author.
E-mail address: jwxiang@wzu.edu.cn (J. Xiang).

https://doi.org/10.1016/j.cep.2022.108862
Received 19 August 2021; Received in revised form 30 January 2022; Accepted 21 February 2022
Available online 26 February 2022

Nomenclature

A	correlation coefficient; membrane area, m^2
B	correlation coefficient
C	correlation coefficient
C_p	heat capacity, $kJ{\cdot}kg^{-1}{\cdot}K^{-1}$
d	hydraulic diameter at the feed bulk solution, m
D	correlation coefficient
e	specific exergy, $kJ{\cdot}kg^{-1}$
E	exergy, kW
h	specific enthalpy, $kJ{\cdot}kg^{-1}$
h_f	heat transfer coefficient through the thermal boundary layer, $W{\cdot}m^{-2}{\cdot}K^{-1}$
I	compression ratio
k	thermal insulation coefficient
K_m	membrane mass transfer coefficient, $kg{\cdot}m^{-2}{\cdot}s^{-1}{\cdot}Pa^{-1}$
l	characteristic constant
M	mass flow rate, $kg{\cdot}s^{-1}$
M_m	molecular weight of water
N	membrane flux, $kg{\cdot}m^{-2}{\cdot}h^{-1}$
Nu	Nusselt number
P	pressure, kPa
Pr	Prandtl number
Q_f	heat flux through the thermal boundary layer, $W{\cdot}m^{-2}$
Q_m	heat flux across the membrane, $W{\cdot}m^{-2}$
r	membrane pore size, μm
R	ideal gas constant, $J{\cdot}mol^{-1}{\cdot}℃^{-1}$
Re	Reynolds number
S	condensate weight, kg
t	centigrade temperature, ℃
T	thermodynamic temperature, K
v	flow velocity, $m{\cdot}s^{-1}$
W	power, W
X	mass concentration
x	mole fraction
y	characteristic constant
z	characteristic constant
ΔH	enthalpy of evaporation for water molecule, $kJ{\cdot}kg^{-1}$

Abbreviation

AGMD	air gap membrane distillation
DCMD	direct contact membrane distillation
SGMD	sweeping gas membrane distillation
SHEC	specific heating energy consumption
VMD	vacuum membrane distillation

Greek letters

δ	thickness, m
ε	porosity
η	efficiency
λ	thermal conductivity, $W{\cdot}m^{-1}{\cdot}℃^{-1}$
μ	dynamic viscosity, $Pa{\cdot}s^{-1}$
ρ	density, $kg{\cdot}m^{-3}$
τ	tortuosity
ψ	separation efficiency
γ	conductivity, $\mu S{\cdot}cm^{-1}$

Subscripts

a	absorb
B	boundary layer
c	chemical; conduction heat
com	compressor
dcom	destruction of compressor
dhex	destruction of heat exchanger
dpum	destruction of pump
dVMD	destruction of VMD module
e	environment
exe	exergy
f	feed side
fm	membrane surface in feed side
g	gas
hex	heat exchanger
in	input
m	membrane; material
me	mechanical
mo	motor
out	output
p	physical; produced condensate
pum	pump
r	release
s	sulfuric acid
sm	saturated state at the membrane surface
sp	saturated state in permeate side
T	total
th	thermal
VMD	vacuum membrane distillation
w	water
wm	water molecule in the solution of membrane surface

molecules from the feed solution. According to the condensation pattern of vapors on the permeate side, MD has four different types: direct contact MD (DCMD) is the earliest and more studied MD process, air gap MD (AGMD) is another MD process characterized by the existence of a certain thickness of air gap, and then sweeping gas MD (SGMD) has been developed and characterized by the injection of inert gas [6,7]. Recently, vacuum MD (VMD) has attracted substantial attention worldwide because of the higher driving force and membrane flux resulting from the vacuum environment applied to the permeate side.

To date, numerous researchers from all over the world have employed the MD technology to deal with sulfuric acid solution and obtained some achievements. Kesieme [8] focused on the application of a DCMD system in the sulfuric acid solution treatment and realized a separation efficiency of nearly 99.9%. Li [9] conducted a test study on the sulfuric acid solution treatment by an AGMD system and attained a higher discharge concentration of 40% at a feed concentration of 2%. In addition, Zhang [10] introduced a VMD device into the field of sulfuric acid solution treatment and achieved a perfect separation efficiency of 100% using this device. Clearly, the abovementioned findings validate that the VMD technology has significant potential in sulfuric acid solution treatment process as compared to those of other methods. However, huge thermal energy is consumed to complete VMD of the sulfuric acid solution owing to the lack of latent heat recovery unit for secondary vapors. Accordingly, how to reduce the energy expenditure of VMD are urgent issues that need to be solved.

Mechanical vapor recompression (MVR), which can effectively utilize internal sensible and latent heat via compression from the compressor, has attracted extensive attention in the past few decades. MVR requires only small amounts of electric energy to provide heat for the evaporation and concentration of initial solution [11,12]. Ai [13] proposed a MVR system to evaporate the sodium chloride solution with high concentrations. Influences of input parameters on the evaporation performance of this system were investigated via numerical simulation. Moreover, the compressor power required to evaporate a ton of water was experimentally determined to be 16.8 kWh under the following conditions: suction pressure: 25 kPa; solution concentration: 18%; and

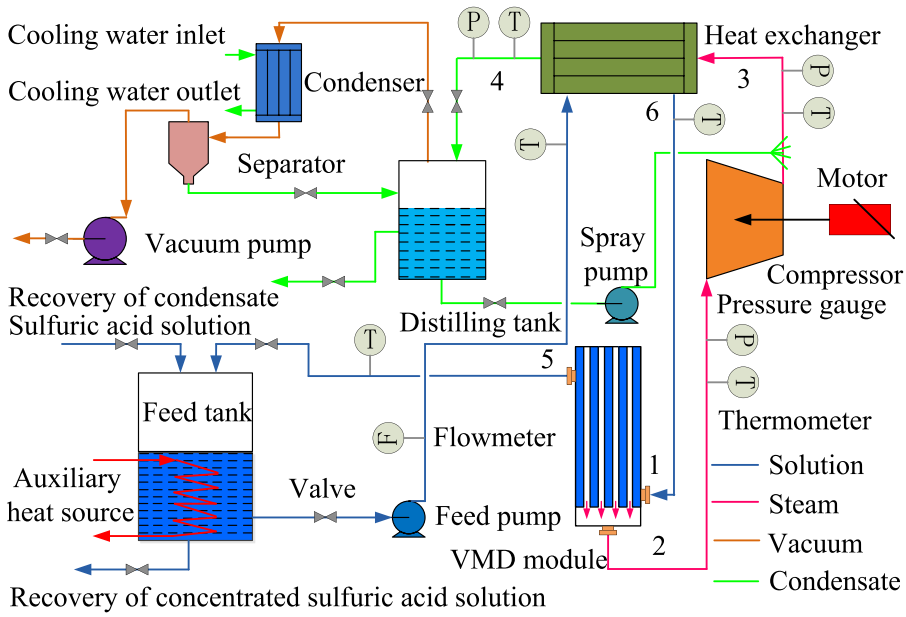

Fig. 1. Schematic of VMD-MVR.

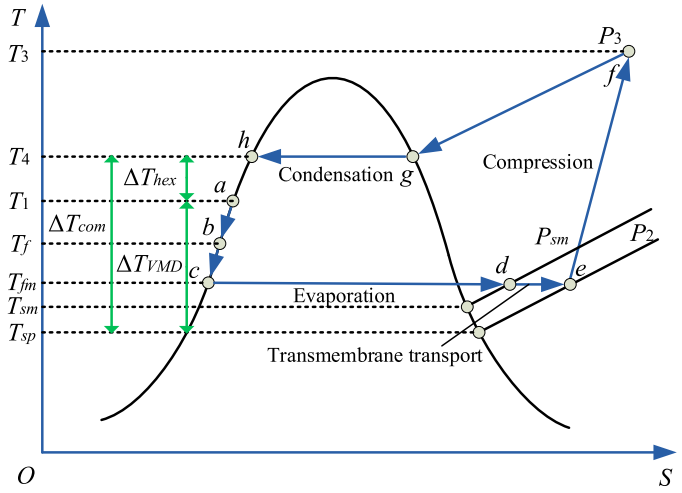

Fig. 2. Diagram of the thermal processes within VMD-MVR.

compressor frequency: 100 Hz. Liang [14] designed and examined a two-effect MVR system to deal with industrial wastewater. The obtained results indicated a 29.2% improvement in the energy efficiency of the two-effect MVR system as compared to that of a single-effect MVR system. Clearly, MVR can be effectively applied to improve the energy conversion efficiency of an evaporation system. However, the weak corrosion resistance and lower separation efficiency caused by the use of a conventional screen and cyclone separator hinder the application of the existing MVR systems in the treatment of strong corrosive solutions.

Based on the abovementioned studies, it is found that the integration of VMD and MVR systems will be a novel concept in the sulfuric acid waste treatment as the VMD system will ensure high-purity separation and the MVR system will result in high-efficiency energy conservation. Apparently, the coupled system has been proven to be useful in resolving the problems of lower separation efficiency, poor operation stability and higher energy consumption in the evaporation and concentration of sulfuric acid waste. Nevertheless, research on this coupled system is still in its infancy; some studies have mainly focused on theoretical analysis and pure water experiment, and the application of this system in the sulfuric acid solution treatment has not been comprehensively analyzed.

Therefore, considering the results of previous studies, this study was aimed to treat sulfuric acid solution by a VMD system based on MVR (VMD-MVR). At first, mathematical models were established and then validated via a VMD-MVR experimental platform using sulfuric acid solution as feed. Thereafter, the performance of VMD-MVR was investigated by the following experimental and simulation methods: (1) Energy and exergy analysis was performed based on the actual operation data utilizing sulfuric acid solution as evaporation object. (2) Effects of several critical parameters, such as feed concentration, feed temperature, feed velocity, permeate side pressure, and heat transfer temperature difference of heat exchanger on the compression and condensation heat transfer of secondary vapors were examined via numerical simulation. (3) Influences of the abovementioned parameters on exergy destruction within VMD-MVR were also simulated and analyzed. The research method proposed herein and the results of this study provide an important reference to optimize the current VMD-MVR system.

2. Experiment

Fig. 1 showed a VMD-MVR system which was made up of feed pump, VMD module, heat exchanger, compressor, feed tank, distilling tank, spray pump, and vacuum system. The VMD module consisted of several membrane tubes, which had high corrosion resistance and were composed of polytetrafluoroethylene (PTFE) microporous membranes. The vacuum system mainly included a vacuum pump, a separator, and a condenser. The initial solution was first heated to a fixed temperature using an auxiliary heat source and then introduced into the heat exchanger to exchange heat with the secondary vapors via the feed pump; subsequently, the solution entered the VMD module, contacting the PTFE microporous membranes. Hence, mass and heat transfer occurred from the bulk solution to the membrane surface through the boundary layer, and the phenomenon of phase change started on the membrane surface. After VMD, the generated vapors diffused to the permeate side because of the transmembrane driving pressure difference, whereas the concentrated solution flowed out of the VMD module and returned to the feed tank for circular concentration. Thereafter, the vapors entered the compressor for compression, during which their saturation temperature and pressure simultaneously increased, and then, the vapors condensed into liquid in the heat exchanger, increasing the temperature of the solution. Finally, the obtained condensate was stored into the distilling tank. Schematic diagram of the entire thermal

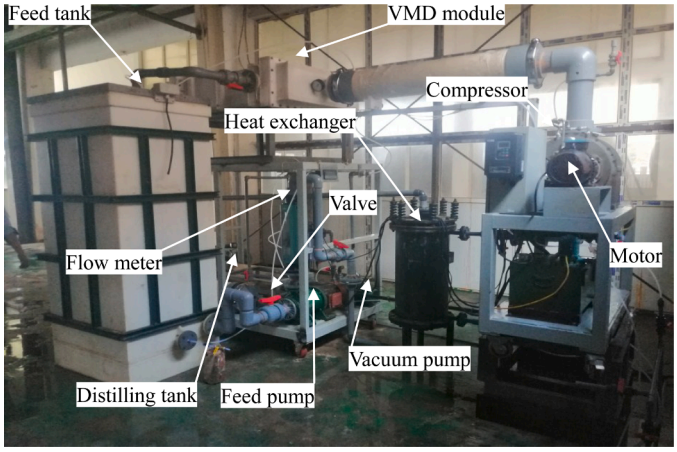

Fig. 3. Experimental platform of VMD-MVR.

Table 1
Performance parameters of the components within the VMD-MVR system.

Components	Types	Parameters	Manufacturers
VMD module	/	Pore size: 0.2 um Membrane area: 20 m^2 Material: PTFE	Nanjing Langtian, Jiangsu
Compressor	LC003	Power: 3 kW	Leke Energy saving, Jiangsu
Heat exchanger	YKC35	Heat transfer area: 4 m^2 Material: Graphite	Nantong Jinsanjiao graphite, Jiangsu
Feed pump	CQB65-50-125F	Power: 4 kW	Jiangnan pump and valve, Anhui
Vacuum pump	2BV2060	Power: 0.81 kW	Boshan Daming, Shandong

process within VMD-MVR according to the integration relationship is presented in Fig. 2, in which *a-b-c-d-e* represents evaporation occurring in the VMD module, *e-f* represents compression taking place in the compressor, and *f-g-h* denotes condensation occurring in the heat exchanger.

A VMD-MVR experimental platform was constructed to demonstrate the feasibility of coupling system, as shown in Fig. 3. The electric heater was utilized as an auxiliary heat source to provide the heat energy required for VMD. Owing to the high corrosivity and risk from the sulfuric acid solution used in this experiment, mostly, anti-corrosive components were used in VMD-MVR. In particular, the feed tank, pipe, and valve were produced from a chlorinated polyvinyl chloride material that could resist the corrosion of sulfuric acid. In addition, the measurement system, including a flow meter, temperature sensor, and pressure sensor, was reformed to increase its anticorrosion performance by coating its components with a PTFE material having high corrosion resistance. The flow meter was used to measure the flow rate at the VMD module inlet, which was in the range of 8–40 $m^3 \cdot h^{-1}$ with a precision of ±2.5%. The temperature sensor was utilized to obtain the temperature of the working fluid at each measurement point, which was in the range of 273.15–373.15 K with a precision of ±1.5%. The pressure sensor was employed to measure the pressure of the working fluid at each measurement point, which was in the range of −0.1–0 MPa with a precision of ±1.0%. Furthermore, a clamp meter was used to evaluate the powers of the compressor and feed pump, which had a precision of ±2.5%. An electronic balance was employed to determine the condensate weight, which had a precision of ±0.1 g. A portable conductivity meter was utilized to determine the conductivity of the working fluid, which had a precision of ±2%. Detailed performance parameters of the components within the VMD-MVR system are presented in Table 1.

3. Theory

In order to simulate the relevant performance of VMD-MVR, the mathematical models are set up in the light of mass and energy conservation principles as well as relevant thermal equilibrium theory, and the relevant assumptions are listed as follows [15–17]:

(1) Heat transfer between the system and surroundings is not considered.
(2) The effect of fouling resistance on heat exchanger is not considered.
(3) Pressure drop from the pumps are neglected.
(4) The produced condensate is the saturated liquid phase.
(5) Membrane fouling and wetting are not considered.

3.1. Physical properties of study object

Taking the sulfuric acid solution as study object, the relevant physical parameters are obtained by fitting on the basis of the experimental data in the literature [18]. The density (ρ) can be gained as follows:

$$\rho = A + BX + CX^2 + DX^3 \quad (1)$$

$$A = 1017.14167 - 2.447 \times 10^{-2}t - 5.68 \times 10^{-3}t^2 - 1.53266 \times 10^{-5}t^3$$

$$B = 4.58895 - 3.35 \times 10^{-2}t + 3.51152 \times 10^{-4}t^2 - 1.20356 \times 10^{-6}t^3$$

$$C = 9.502 \times 10^{-2} + 4.4563 \times 10^{-4}t - 5.88 \times 10^{-6}t^2 + 2.7729 \times 10^{-8}t^3$$

$$D = -5.0676 \times 10^{-4} - 2.34115 \times 10^{-6}t + 2.97124 \times 10^{-8}t^2 - 1.27254 \times 10^{-10}t^3$$

The specific heat capacity (C_p) can be obtained as follows:

$$Cp = A + BX + CX^2 + DX^3 \quad (2)$$

$$A = 4127.00244 - 2.92176t + 8.371 \times 10^{-2}t^2 - 5.74437 \times 10^{-4}t^3$$

$$B = -17.76172 - 0.13005t + 2.93842 \times 10^{-4}t^2 - 4.85811 \times 10^{-6}t^3$$

$$C = -0.54749 + 4.42 \times 10^{-3}t + 3.65572 \times 10^{-6}t^2 - 4.77794 \times 10^{-8}t^3$$

$$D = 5.16 \times 10^{-3} - 2.82683 \times 10^{-5}t - 2.34475 \times 10^{-7}t^2 + 2.67415 \times 10^{-9}t^3$$

The dynamic viscosity (μ) can be written as follows:

$$\mu = A + BX + CX^2 + DX^3 \quad (3)$$

$$A = -1.65529 + 0.10614t - 1.8 \times 10^{-3}t^2 + 1.00108 \times 10^{-5}t^3$$

$$B = 0.60288 - 2.614 \times 10^{-2}t + 4.0464 \times 10^{-4}t^2 - 2.1597 \times 10^{-6}t^3$$

$$C = -2.234 \times 10^{-2} + 1.01 \times 10^{-3}t - 1.6182 \times 10^{-5}t^2 + 8.88519 \times 10^{-8}t^3$$

$$D = 2.63986 \times 10^{-4} - 1.15723 \times 10^{-5}t + 1.87223 \times 10^{-7}t^2 - 1.04567 \times 10^{-9}t^3$$

The thermal conductivity (λ) can be expressed as follows:

$$\lambda = A + BX + CX^2 + DX^3 \quad (4)$$

$$A = 0.51427 + 2.08 \times 10^{-3}t - 1.00125 \times 10^{-5}t^2 + 6.66667 \times 10^{-8}t^3$$

$$B = -1.6 \times 10^{-3} - 8.55595 \times 10^{-5}t + 1.78036 \times 10^{-6}t^2 - 1.20833 \times 10^{-8}t^3$$

$$C = -2.58869 \times 10^{-5} + 2.10036 \times 10^{-6}t - 4.83941 \times 10^{-8}t^2 + 3.3054 \times 10^{-10}t^3$$

$$D = 1.81395 \times 10^{-7} - 1.47133 \times 10^{-8}t + 3.39987 \times 10^{-10}t^2 - 2.32779 \times 10^{-12}t^3$$

where *A*, *B*, *C* and *D* represent the related coefficients, respectively. *t* represents the solution temperature. *X* represents the

mass concentration of solution.

3.2. VMD module

As one of the core devices within the entire system, the VMD module is applied to evaporate the feed sulfuric acid solution, the relevant mass and energy balance in which are acquired as follows:

$$M_1 = M_2 + M_5 \tag{5}$$

$$M_1X_1 = M_5X_5 \tag{6}$$

$$M_1h_1 = M_2h_2 + M_5h_5 \tag{7}$$

where h_1, M_1 and X_1 represent the specific enthalpy, mass flow rate and concentration of the inlet solution, respectively. h_5, M_5 and X_5 represent the specific enthalpy, mass flow rate, concentration of the outlet concentrated solution, respectively. h_2 and M_2 represent the specific enthalpy and mass flow rate of the outlet vapor, respectively.

Mass and heat transfer, from the bulk solution to the hot side membrane surface across the boundary layer, arise simultaneously in the VMD process, and the transferred heat (Q_f) can be expressed as follows [19]:

$$Q_f = h_f\left(T_f - T_{fm}\right) \tag{8}$$

where T_{fm} represents membrane surface temperature. T_f represents the bulk solution temperature, which can be expressed as follows:

$$T_f = \frac{T_1 + T_5}{2} \tag{9}$$

The heat transfer coefficient, h_f, is given by:

$$h_f = \frac{y\lambda \mathrm{Re}^l \mathrm{Pr}^z}{d} \tag{10}$$

where l, y and z represent characteristic constants, respectively. d represents the hydraulic diameter. Re represents the Reynolds number and Pr represents the Prandtl number, which can be expressed as follows:

$$Re = \frac{vd\rho}{\mu} \tag{11}$$

$$Pr = \frac{C_p\mu}{\lambda} \tag{12}$$

where v is the feed velocity.

In general, the heat conduction across the membrane is not considered owing to the higher vacuum degree applied in the permeate side [20]. Accordingly, the heat transfer (Q_m) across the membrane is expressed as follows:

$$Q_m = N\Delta H \tag{13}$$

where N and ΔH represent the membrane flux and evaporation enthalpy of the water molecule, respectively.

As a result, the heat transfer equation in the VMD process based on the energy conservation is given by:

$$h_f\left(T_f - T_{fm}\right) = N\Delta H \tag{14}$$

In addition, mass transfer always occurs with heat transfer in the VMD process, the corresponding mass transfer equation is expressed as follows [21,22]:

$$N = K_m\Delta P = \left[1.064\frac{r\varepsilon}{\tau\delta}\left(\frac{M_m}{RT_m}\right)^{1/2} + 0.125\frac{r^2\varepsilon}{\tau\delta}\left(\frac{M_mP_m}{\mu_vRT_m}\right)\right]\Delta P \tag{15}$$

where K_m, M_m, r, R, ε, δ and τ represent the mass transfer coefficient, water molecular weight, membrane pore size, ideal gas constant, membrane porosity, membrane thickness and membrane tortuosity, respectively. T_m represents the average membrane pore temperature and P_m represents the average membrane pore pressure. The driving pressure difference (ΔP) is expressed as follows:

$$\Delta P = P_{sm} - P_2 = \left(x_{wm}\left(1 - 0.5x_{fm} - 10x_{fm}^2\right)\right)P_{fm} - P_2 = \left(x_{wm}\left(1 - 0.5x_{fm} - 10x_{fm}^2\right)\right)\exp\left(23.238 - \frac{3841}{T_{fm} - 45}\right) - P_2 \tag{16}$$

where xfm and xwm represent the mole fractions of sulphuric acid and water, respectively. Pfm represents the saturated vapor pressure of the pure water with a temperature of Tfm.

In the VMD process, the transfer resistance of water molecule in the heat and mass transfer process from the bulk solution to the permeate side is relatively complex. In order to simplify the model, the total resistance (R_T) is mainly divided into two parts. The first part is the obstruction from the hot side boundary layer, which can be calculated as follows:

$$RB = \frac{P_f - P_{sm}}{N} \tag{17}$$

The other part is the resistance from the membrane itself, which can be expressed as follows:

$$R_m = \frac{P_{sm} - P_2}{N} \tag{18}$$

where RB and Rm represent the boundary layer resistance and membrane resistance, respectively.

3.3. Compressor

The compressor is put into application to increase the saturated temperature and pressure of the secondary vapor from the VMD module by the compression process. The temperature of vapor at the compressor outlet can be expressed as follows:

$$T_3 = T_2(I)^{\frac{k-1}{k}} = T_2\left(\frac{P_3}{P_2}\right)^{\frac{k-1}{k}} \tag{19}$$

where T_2, P_2, T_3 and P_3 are the inlet temperature, inlet pressure, outlet temperature and outlet pressure, respectively. k and I are the thermal insulation coefficient and compression ratio, respectively.

The compressor power is described as follows [23]:

$$W_{com} = \frac{(h_3 - h_2)M_2}{\eta_{th}\cdot\eta_{me}\cdot\eta_{mo}} \tag{20}$$

where h_2 and h_3 represent the specific enthalpies of the vapor at the compressor inlet and outlet, respectively. η_{me}, η_{mo} and η_{th} represent the mechanical, motor and thermal efficiencies, respectively.

For the current VMD-MVR system, the compressor power is mainly determined by the difference of saturation temperature between inlet and outlet (ΔT_{com}), it is seen from Fig. 2 thatΔT_{com} can be calculated as follows:

$$\Delta T_{com} = \Delta T_{hex} + \left(T_1 - T_{sp}\right) = \Delta T_{hex} + \Delta T_{VMD} \tag{21}$$

where T_{sp} represents saturated temperature of vapor under the pressure of P_2. ΔT_{hex} represents the heat tranfer temperature difference of heat exchanger.ΔT_{VMD} represents the temperature difference between inlet solution and outlet saturated vapor under the pressure of P_2, which is affected by many factors, containing feed concentration, boundary resistance, temperature polarization effect, concentration polarization effect and membrane resistance.

3.4. Heat exchanger

The heat exchanger is utilized to recover the latent heat of secondary vapor and heat the sulfuric acid solution simultaneously. As a consequence, the corresponding energy equilibrium equation can be expressed as follows [24]:

$$M_5(h_6 - h_5) = M_3(h_3 - h_4) \tag{22}$$

M_3, h_4 and h_6 are the mass flow rate of vapor at the heat exchanger inlet, specific enthalpy of condensate at the heat exchanger outlet and specific enthalpy of solution at the heat exchanger outlet, respectively.

3.5. Exergy

Exergy has always been introduced to assess the quality of energy in practical engineering. In general, exergy shows a decreasing trend in the conversion process resulted from the elevation of entropy caused by irreversible factors. Exergy analysis method can be used to analyze the coupled system by comprehensively considering the first and second laws of thermodynamics. In this section, for the convenience of exergy analysis and calculation, the reference parameters including ambient temperature, pressure and solution concentration are set at 298.15 K, 0.1 MPa and 5%, respectively. Exergy is usually divided into two kinds, one is the physical exergy and the other is the chemical exergy [25]. The logistics within the current coupled system mainly includes sulfuric acid solution, water and vapor. For the aspect of water and vapor, the chemical exergy can be ignored without considering the impacts from concentration, and only physical exergy is considered, and the calculation formula is as follows:

$$e_p = (h - h_0) - T_0(s - s_0) \tag{23}$$

where e_p is the specific physical exergy. T_0 is the temperature of water or vapor at the ambient reference state. h_0 and h are the specific enthalpy of water or vapor at the ambient reference state and calculated state, respectively. s_0 and s are the specific entropy of water or vapor at ambient reference state and calculated state, respectively.

The sulfuric acid solution used in this study can be assumed to be an ideal solution mixed with sulfuric acid and pure water. Its specific exergy, e, can be expressed as follows:

$$e = e_p + e_c \tag{24}$$

$$e_p = C_p(T - T_0 - T_0 \ln(T / T_0)) \tag{25}$$

$$e_c = T_0(R_s X_s \ln(x_s / x_{s0}) + R_w X_w \ln(x_w / x_{w0})) \tag{26}$$

where e_p is the specific physical exergy. e_c is the specific chemical exergy. x_s and X_s are the molar and mass fractions of sulfuric acid at the calculated state, respectively. x_w and X_w are the molar and mass fractions of water at the calculated state, respectively. x_{s0} and x_{w0} are the molar fractions of sulfuric acid and water at the reference state.

In addition, exergy destruction reflects the irreversible degree of the actual thermodynamic process. The greater the exergy destruction, the higher the irreversibility degree. After determining the exergy values of working fluid at different positions within the entire system, the exergy destruction needs to be further evaluated. The exergy destruction of the VMD module can be expressed as follows:

$$E_{dVMD} = M_1 e_1 - M_5 e_5 - M_2 e_2 \tag{27}$$

where e_1, e_2 and e_5 represent the specific exergies of inlet solution, outlet vapor and outlet solution, respectively.

The exergy destruction of heat exchanger can be expressed as follows:

$$E_{dhex} = M_2 e_3 + M_5 e_5 - M_2 e_4 - M_5 e_1 \tag{28}$$

where e_3 and e_4 represent the specific exergies of inlet vapor and outlet condensate, respectively.

The exergy destructions of compressor and feed pump can be expressed as follows:

$$E_{dcom} = (1 - \eta_{mo}) W_{com} + (1 - \eta_{com}) \eta_{mo} W_{com} \tag{29}$$

$$E_{dpum} = (1 - \eta_{mo}) W_{pum} + \frac{T_0}{T_{pum}} (1 - \eta_{pum}) W_{pum} \tag{30}$$

where η_{com}, η_{pum} and T_{pum} are compressor efficiency, feed pump efficiency and solution temperature through the feed pump, respectively. W_{pum} represents the feed pump power, which is given as follows:

$$W_{pum} = \frac{M_1 \rho g}{3.6 \times 10^6 \eta_{pum}} \left(\Delta Z + \frac{v^2}{2g} \right) \tag{31}$$

where g and ΔZ represent the gravity acceleration and feed pump lift, respectively.

However, exergy destruction is only a numerical value and does not reflect the utilization degree of exergy in the thermal process. Therefore, exergy efficiency is introduced in the thermal analysis process, which is a completeness indicator of the thermodynamic process within the system. For the VMD-MVR system, the exergy efficiency is the ratio of exergy output and exergy input, the exergy input is the sum of compressor power and pump power, and the energy output is the sum of enthalpy for the condensate and concentrate solution. The exergy efficiency is given by:

$$\eta_{exe} = \frac{E_{out}}{E_{in}} \times 100\% \tag{32}$$

3.6. Performance evaluation criterion

The membrane flux in the experiment process is written as [26]:

$$N = \frac{S}{A \times t} \tag{33}$$

where S, A and t represent the condensate weight, membrane area and sampling time, respectively.

The separation efficiency (ψ) of the system is expressed as follows [27]:

$$\psi = \left(1 - \frac{\gamma_p}{\gamma_f} \right) \times 100\% \tag{34}$$

where γ_p and γ_f represent the conductivities of the produced condensate and feed solution, respectively.

Performance coefficient (COP) for the VMD-MVR system can be described as follows [28]:

$$COP = \frac{(h_3 - h_4) M_2}{W_{com}} \tag{35}$$

The thermal efficiency in the VMD process, η_{VMD}, is defined as follows:

$$\eta_{VMD} = \frac{Q_m}{M_1 h_1 - M_5 h_5} \times 100\% = \frac{Q_m}{Q_m + Q_e + Q_c} \times 100\% \tag{36}$$

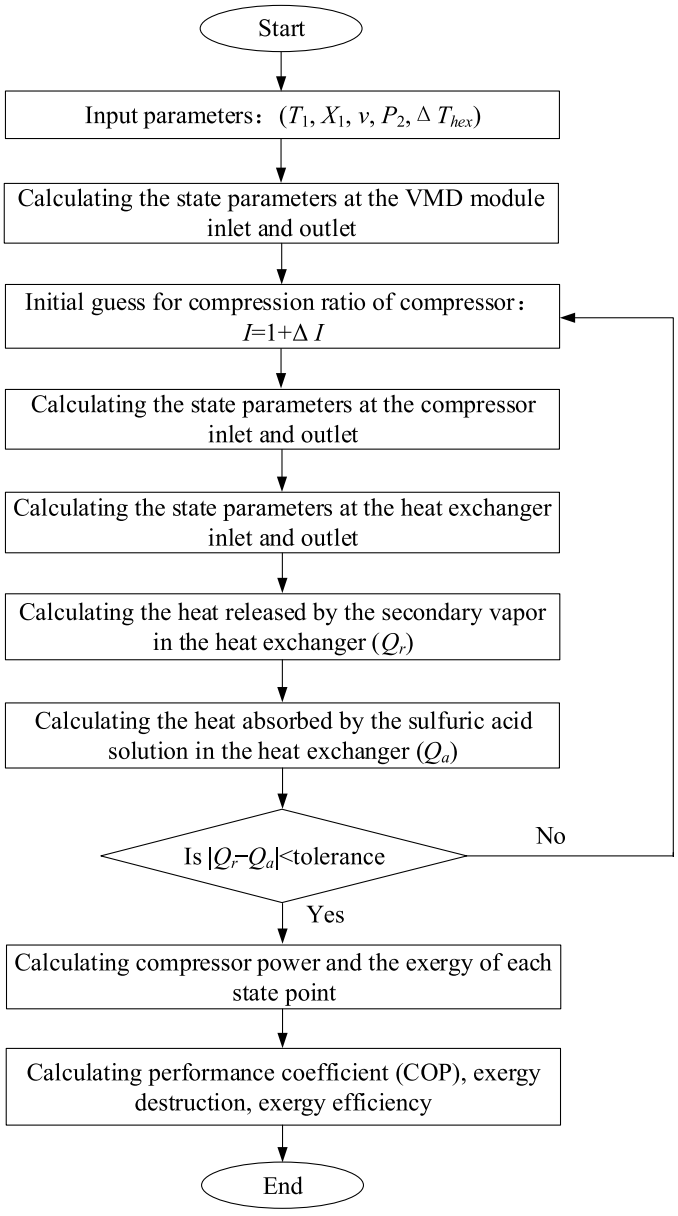

Fig. 4. Solving procedure in the simulation process.

Table 2
Verification results of the mathematical models.

Parameters	Simulated value	Experimental value
X_1/%	5	5
T_1/K	353.0	353.0
v /m·s^{-1}	1.6	1.6
P_2/kPa	45	45
T_5/ K	352.7	351.8
T_2 / K	352.8	351.0
T_3/ K	355.2	355.5
T_4/K	355.2	355.0
N/ kg·m^{-2}·h^{-1}	2.26	1.70

where Q_e is the heat loss to the environment for the VMD module, Q_c is the transmembrane heat conduction, which is expressed as follows:

$$Q_c = A\left((1-\varepsilon)\lambda_m + \varepsilon\lambda_g\right)\left(T_{fm} - T_2\right)/\delta \quad (37)$$

where λ_m is the thermal conductivity of membrane material, λ_g is the thermal conductivity of gas within the membrane pore.

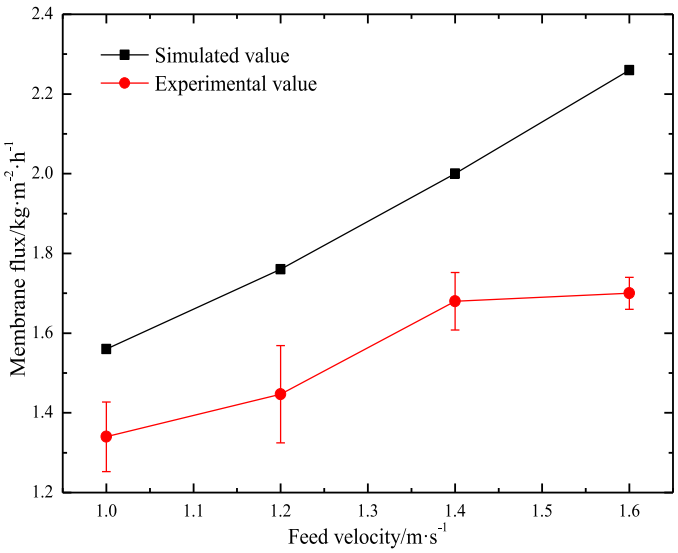

Fig. 5. Comparison of the simulated and experimental values.

Via the established mathematical models of VMD-MVR, the performance of VMD-MVR is simulated by repeatedly solving the equilibrium equations using Matlab software, and the detailed solving procedure in the simulation process is depicted in Fig. 4.

4. Results and discussion

4.1. Experiment of the coupling of VMD with MVR

4.1.1. Model validation

In this section, the experimental results acquired via VMD-MVR using actual sulfuric acid solution as feed were employed to verify the accuracy and reliability of the current mathematical models Table 2. showed a comparison results of the simulated and experimental values, at the conditions of feed temperature of 353 K, feed concentration of 5%, feed velocity of 1.6 m·s^{-1}, and permeate side pressure of 45 kPa, the maximum deviation with a value of 24.8% was obtained for the membrane flux, whereas the corresponding deviations for other parameters were below 10%. Furthermore, membrane fluxs of simulation and experiment under different feed velocities were compared in the Fig. 5, at the conditions of feed temperature of 353 K, feed concentration of 5%, and permeate side pressure of 45 kPa, it was observed that the deviation varied from 14.1% to 24.8% as feed velocity increased from 1.0 m·s^{-1} to 1.6 m·s^{-1}. Considering that our team first carried out research on MVR coupled with VMD, due to limited resources and lack of experience, the used VMD module was folding tubular membrane with higher membrane thickness, resulting in large errors between simulated and experimental membrane flux. Nevertheless, the deviations for other parameters was acceptable. Therefore, the limited deviations between the simulated and experimental values could confirm the accuracy and reliability of the established mathematical models.

4.1.2. Analysis of operation stability

The long-term operation stability of the VMD-MVR system should be first investigated Fig. 6. showed the each point temperature and pressure with operation time from 0 to 120 min at the conditions of feed concentration of 5%, feed temperature of 353.0 K and feed velocity of 1.6 m·s^{-1}. Firstly, the pressures at the compressor inlet and outlet were reduced from 100 kPa to 40 kPa by vacuumizing. Then, the pressure difference between inlet and outlet of compressor was gradually generated due to the compression process. As a result, the temperature of secondary vapor at compressor outlet was increased accordingly, and

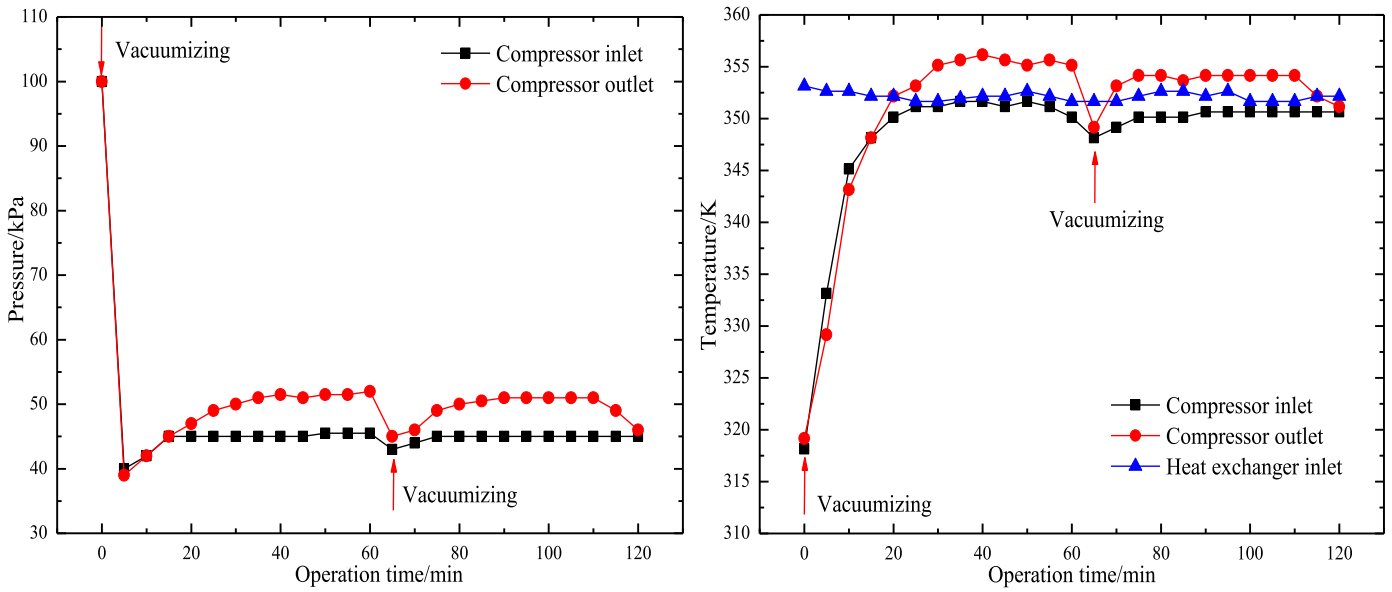

Fig. 6. Each point temperature and pressure with operation time.

Table 3
Membrane flux and condensate conductivity with operation time.

Time/ h	Membrane flux/ $kg{\cdot}m^{-2}{\cdot}h^{-1}$	Conductivity/ $uS{\cdot}cm^{-1}$	Time/ h	Membrane flux/ $kg{\cdot}m^{-2}{\cdot}h^{-1}$	Conductivity/ $uS{\cdot}cm^{-1}$
4	1.72	90	28	1.68	94
8	1.68	92	32	1.7	95
12	1.71	98	36	1.68	97
16	1.69	94	40	1.66	95
20	1.68	92	44	1.67	93
24	1.7	90	48	1.65	94

Table 4
Orthogonal experimental design and results of VMD-MVR.

Test number	Factors				Performance index
	A/T_1	B/X_1	C/v	D/P_2	Membrane flux
1	355.5	10	1.4	37.5	1.97
2	358	2.5	1.4	42.5	2.00
3	360.5	7.5	1.2	37.5	2.31
4	355.5	5	1.0	45	1.74
5	360.5	5	1.4	40	2.31
6	353	10	1.6	40	1.99
7	355.5	2.5	1.2	40	1.99
8	358	7.5	1.0	40	2.10
9	353	7.5	1.4	45	1.68
10	358	10	1.2	45	1.85
11	355.5	7.5	1.6	42.5	2.10
12	353	2.5	1.0	37.5	2.02
13	358	5	1.6	37.5	2.31
14	360.5	10	1.0	42.5	2.14
15	353	5	1.2	42.5	1.76
16	360.5	2.5	1.6	45	2.31
k_{1j}	1.8625	2.0800	2.0000	2.1525	
k_{2j}	1.9500	2.0300	1.9775	2.0975	
k_{3j}	2.0650	2.0475	1.9900	2.0000	
k_{4j}	2.2675	1.9875	2.1775	1.8950	
R	0.4050	0.0925	0.2000	0.2575	
Rank	1	4	3	2	
Optimal level	A_4	B_1	C_4	D_1	
Optimal combination	$A_4B_1C_4D_1$				

Table 5
Logistic parameters of VMD for the treatment of sulfuric acid solution.

Parameter	Value	Parameter	Value
X_1/%	5	R_B/$kPa{\cdot}m^2{\cdot}h{\cdot}kg^{-1}$	0.603
T_1/K	353.0	R_m /$kPa{\cdot}m^2{\cdot}h{\cdot}kg^{-1}$	0.161
v/$m{\cdot}s^{-1}$	1.6	R_T/$kPa{\cdot}m^2{\cdot}h{\cdot}kg^{-1}$	0.764
P_2/kPa	45	K_m /$kg{\cdot}m^{-2}{\cdot}h^{-1}{\cdot}Pa^{-1}$	0.006
T_2 /K	351.0	Q_f /kW	23.176
T_5 /K	351.8	Q_m/kW	21.810
X_5/%	5.008	Q_c/kW	1.366
T_f/K	352.4	Q_e /kW	5.628
X_f /%	5.004	Q_{VMD}/kW	28.804
h_f / $W{\cdot}m^{-2}{\cdot}K^{-1}$	6840	N/ $kg{\cdot}m^{-2}{\cdot}h^{-1}$	1.7
T_{fm} /K	352.2	ψ/%	99.9%
X_{fm} /%	5.04%	η_{VMD} /%	75.72

was higher than that of the temperatures of compressor inlet vapor and heat exchanger inlet solution, which ensured that the secondary vapor could release the latent heat to the solution in the heat exchanger through the condensation process. After 60 min of operation, the system was vacuumized again to ensure stable water production. It was obvious that the system exhibited excellent operation stability during the period of 120 min. In addition, in order to further verify the operation stability, an experiment of continuous operation for 48 h was carried out, Table 3 showed the membrane flux and condensate conductivity with operation time at the conditions of feed concentration of 5%, feed temperature of 353.0 K and feed velocity of 1.6 $m{\cdot}s^{-1}$, it was found that the membrane flux fluctuated between 1.65 to 1.72 $kg{\cdot}m^{-2}{\cdot}h^{-1}$ and condensate conductivity fluctuated between 90 and 98 $uS{\cdot}cm^{-1}$. Apparently, membrane wetting and membrane fouling were not obvious during the operation time. Therefore, the proposed system has a better water production stability and long-term operation stability.

4.1.3. Analysis of orthogonal experiment

In this section, an orthogonal experiment was adopted to investigate the influence of multi-variable on water production and obtain the optimal parameter combination for achieving the maximum water production flux Table 4. showed a $L_{16}(4^4)$ orthogonal array with 16 representative experimental points in the light of the standard orthogonal table, using feed temperature, feed concentration, feed velocity and permeate side pressure as variable factors, and membrane flux as

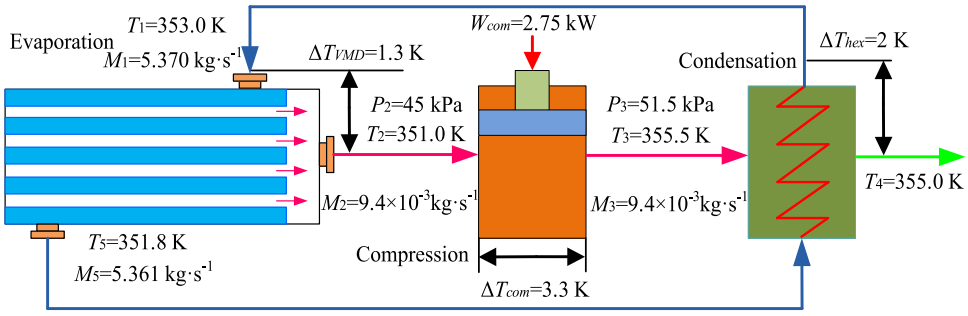

Fig. 7. Internal logistic parameters of VMD-MVR for the treatment of sulfuric acid solution.

Table 6
Exergy performance analysis of VMD-MVR.

Type		Value
Exergy input/kW	Compressor	2.75
	Feed pump	2.2
	Total	4.95
Exergy destruction/kW	VMD module	0.530
	Compressor	1.580
	Heat exchanger	0.895
	Feed pump	1.030
	Other	0.656
	Total	4.691
Exergy output/kW	0.259	
η_{exe} /%	5.24	

Table 7
Detailed design parameters for simulation.

Parameters		Value
Membrane characteristic parameters	r /μm	0.2
	ε/%	80
	A /m^2	20
Operation parameters	X_1/%	5–35
	T_1/K	353.0–363.0
	v/m·s^{-1}	1.0–1.8
	P_2/kPa	5–70
	ΔT_{hex} /K	4–16
Compressor parameters	η_{th} /%	76
	η_{me} /%	80
	η_{mo} /%	70

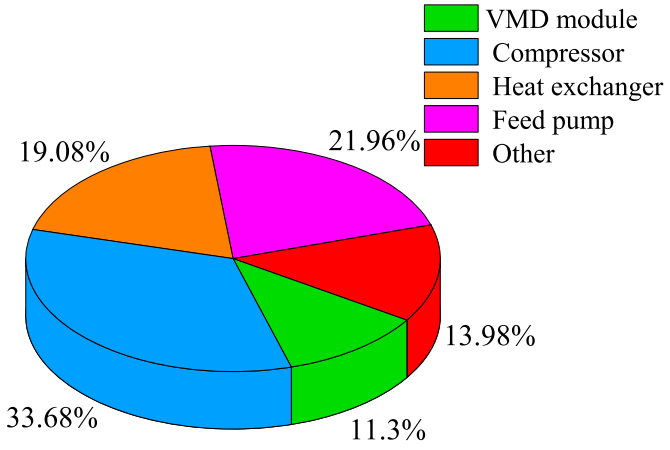

Fig. 8. Exergy destruction distribution in each component of VMD-MVR.

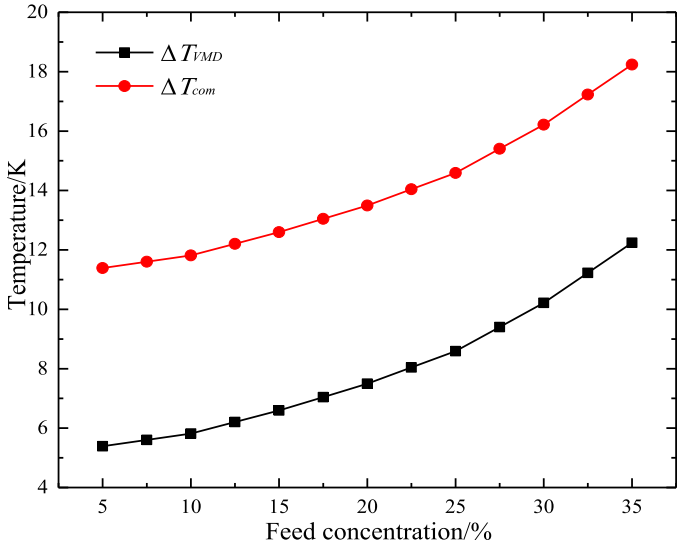

Fig. 9. Effect of feed concentration on ΔT_{VMD} and ΔT_{com}.

experimental index. A range analysis was introduced to analyze the orthogonal experiment results. The deviation between the minimum and maximum of the average values for the various levels of each factor was expressed as the range, R, which could be used to judge the influence of each factor on the experimental index. The greater effect of one factor on experimental index corresponded to a larger value of R. Therefore, the value of R could be employed to rank the importance of the variable factors. It could be seen from the Table 4 that the values of R for each factor were R_1=0.4050, R_2=0.0925, R_3=0.2, R_4=0.2575. The R_1 in the first column was found to be the largest, while the R in the second, third and fourth columns were observed to be smaller, with R_3 being smaller than R_4 but larger than R_2, which indicated that the membrane flux fluctuated most as the factors of *A, C* and *D* varied, but less as the factor of *B* varied. Thus, the order of the factors influencing the membrane flux was ranked as follows: feed concentration (*B*)< feed velocity (*C*)< permeate side pressure (*D*)<feed temperature (*A*). In addition, since experimental index was membrane flux, it was concluded that A_4 was the optimal level of factor *A*. Similarly, for the aspect of factor *B, C* and *D*, the optimal levels were observed to be B_1, C_4 and D_1, respectively. Therefore, the optimal parameter combination was obtained as $A_4B_1C_4D_1$, namely feed temperature of 360.5 K, feed concentration of 2.5%, feed velocity of 1.6 m·s^{-1} and permeate side pressure of 37.5 kPa.

4.1.4. Analysis of energy efficiency

Table 5 presents the logistic parameters of VMD for the concentration of sulfuric acid solution. The membrane flux and separation efficiency were found to be 1.7 kg·m^{-2}·h^{-1} and 99.9% during the stable operation period of 1 h. During VMD of the sulfuric acid solution, water molecules transferred from the bulk sulfuric acid solution to the hot side membrane surface by overcoming the boundary layer resistance,

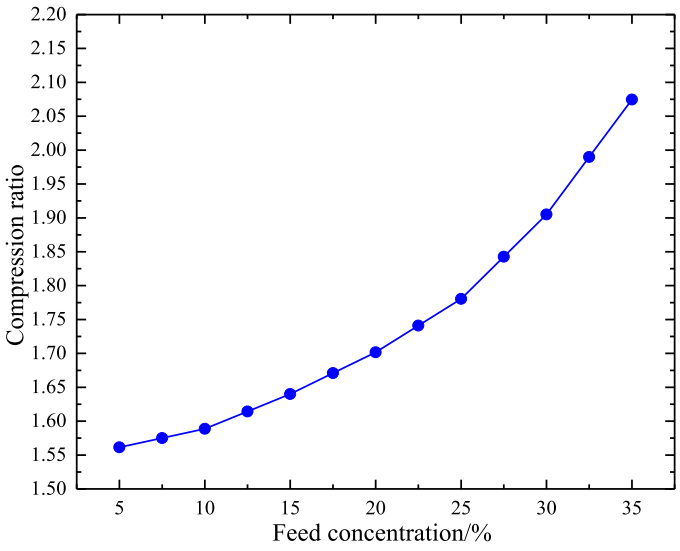

Fig. 10. Effect of feed concentration on compression ratio.

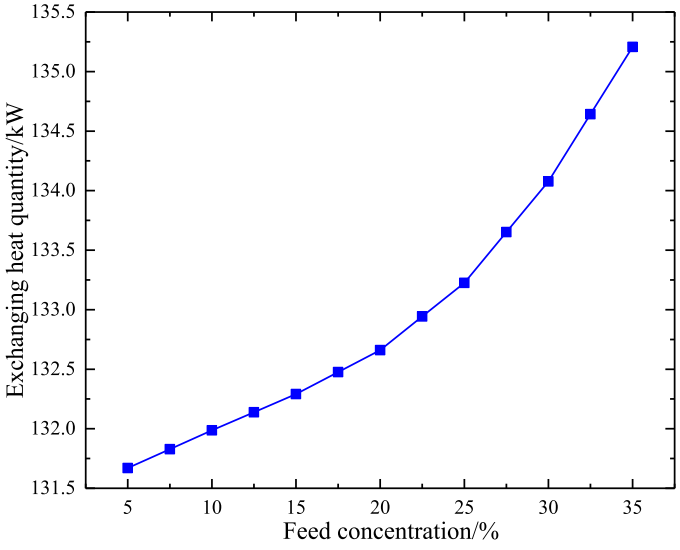

Fig. 11. Effect of feed concentration on exchanging heat quantity.

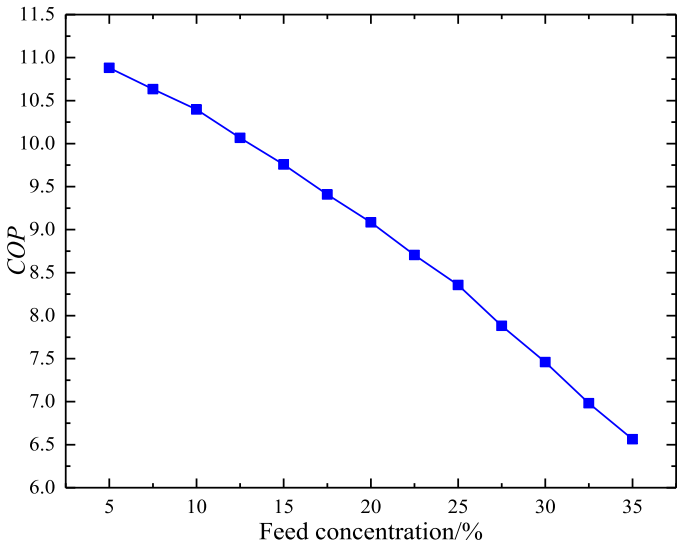

Fig. 12. Effect of feed concentration on *COP*.

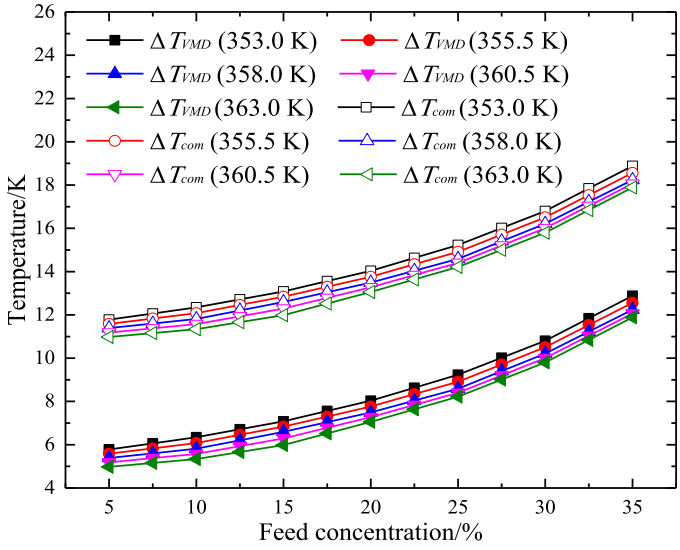

Fig. 13. Effect of feed temperature and feed concentration on ΔT_{VMD} and ΔT_{com}.

evaporated into vapors by absorbing the heat, and then arrived at the permeate side by overcoming the membrane resistance owing to the vapor pressure difference across the membrane. The convective heat transfer coefficient was 6840 $W{\cdot}m^{-2}{\cdot}K^{-1}$, and the transmembrane mass transfer coefficient was 0.006 $kg{\cdot}m^{-2}{\cdot}h^{-1}{\cdot}Pa^{-1}$ (Table 5). In addition, the resistance during VMD was determined to be 0.764 $kPa{\cdot}m^2{\cdot}h{\cdot}kg^{-1}$, comprising a boundary resistance of 0.603 $kPa{\cdot}m^2{\cdot}h{\cdot}kg^{-1}$ and a membrane resistance of 0.161 $kPa{\cdot}m^2{\cdot}h{\cdot}kg^{-1}$. Clearly, as water molecules needed to overcome various resistances to perform heat and mass transfer during VMD, certain temperature and concentration gradients developed during the entire process. The temperatures of the inlet solution, bulk solution, membrane surface solution, and outlet vapor were 353.0, 352.4, 352.2, and 351.0 K, respectively. The concentrations of the inlet solution, bulk solution, and membrane surface solution were 5, 5.004, and 5.04%, respectively. Due to the evaporation of sulfuric acid solution in the VMD module, the temperature of the outlet solution was lower than that of the inlet solution. However, the existence of the boundary layer resistance caused temperature polarization, resulting in a lower temperature of the membrane surface when compared with that of the bulk solution. Generally, transmembrane heat conduction loss is not considered in numerical simulation, and the outlet vapor temperature is believed to be approximately equal to the membrane surface temperature. However, in the actual process, the outlet vapor temperature was lower than the membrane surface temperature owing to the heat conduction loss. Similarly, the concentration of the membrane surface solution was higher than that of the bulk solution, which is called the concentration polarization phenomenon. Consequently, due to the existence of temperature and concentration polarization, the vapor partial pressure at the membrane surface was slightly reduced, and the transmembrane driving force was weakened, leading to the reduction of membrane flux. Therefore, the impacts of temperature and concentration polarization should be reduced during actual VMD.

In addition, the total heat provided by the VMD module was 28.804 kW, in which the latent heat of vaporization, transmembrane heat conduction loss, and heat loss to the environment were 21.810, 1.366, and 5.628 kW, respectively (Table 5). Furthermore, the convective heat transfer was 23.176 kW, which was mainly used for the latent heat of vaporization and transmembrane heat conduction loss. Consequently, a thermal efficiency of 75.72% was obtained for VMD. Clearly, the latent heat of vaporization occupied a large proportion. Once it was recovered and utilized by MVR technology, the energy efficiency of entire VMD

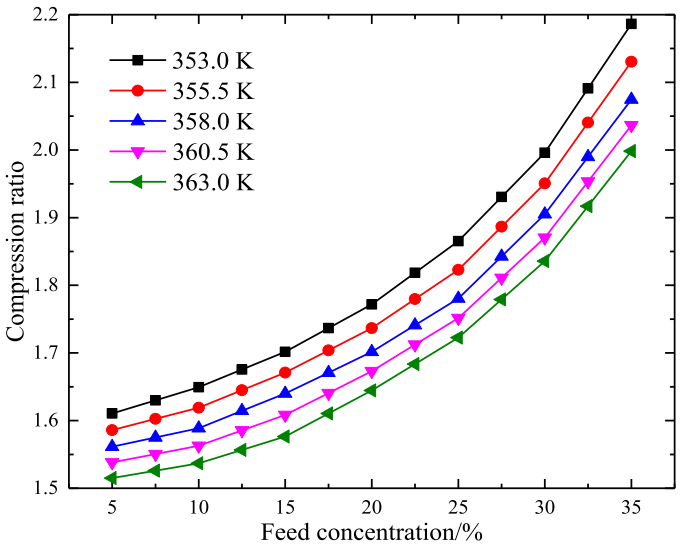

Fig. 14. Effect of feed temperature and feed concentration on compression ratio.

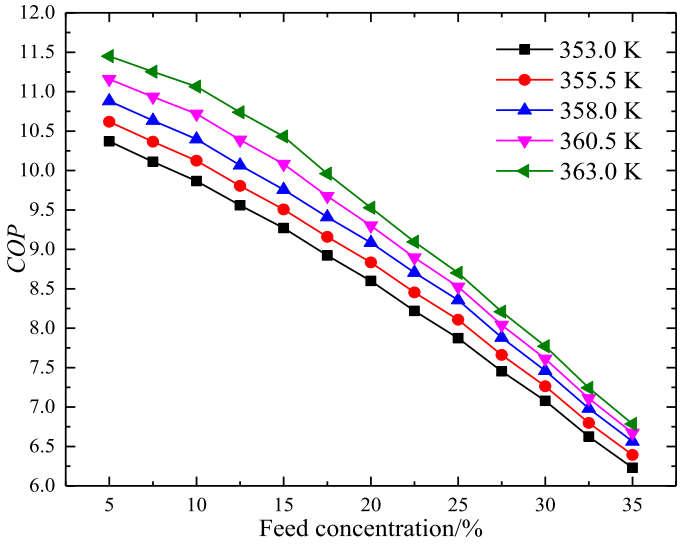

Fig. 16. Effect of feed temperature and feed concentration on *COP*.

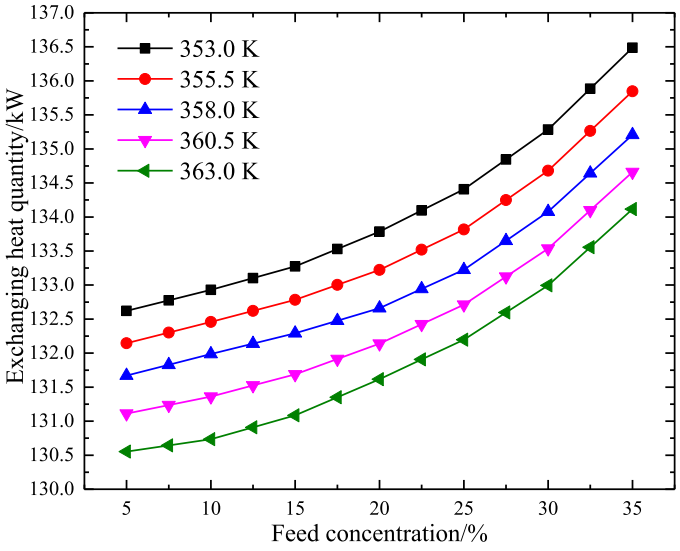

Fig. 15. Effect of feed temperature and feed concentration on exchanging heat quantity.

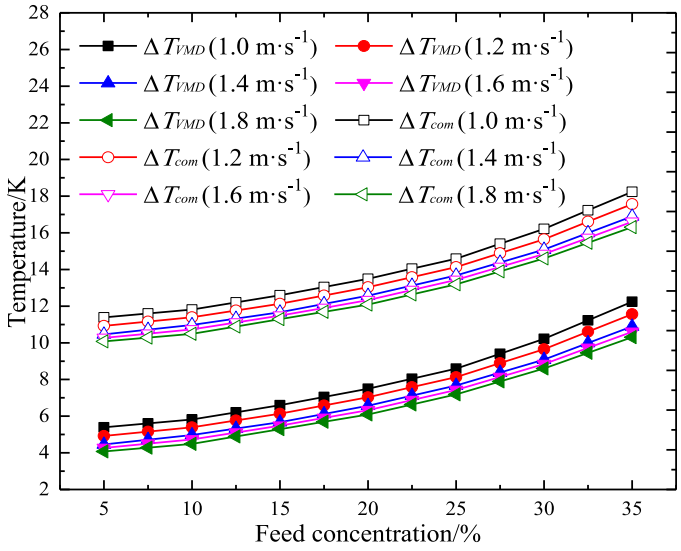

Fig. 17. Effect of feed velocity and feed concentration on ΔT_{VMD} and ΔT_{com}.

was significantly enhanced Fig. 7. shows the internal logistic parameters of VMD-MVR in sulfuric acid solution treatment process, and ΔT_{VMD}, ΔT_{hex}, and ΔT_{com} were calculated to be 1.3, 2, and 3.3 K, respectively, when the compressor frequency was fixed at 40 Hz. The corresponding pressures at the compressor inlet and outlet were 45 and 51.5 kPa, and the compression ratio was 1.13. Moreover, the compressor power was determined to be 2.75 kW by measuring the current and voltage of the motor employed to drive the compressor. Thus, the *SHEC* and performance coefficient (*COP*) were calculated to be 80.88 kWh·t^{-1} and 7.88, respectively. Apparently, the latent heat of the secondary vapors produced during VMD was effectively recovered by MVR. When the insulation of the system components and pipelines was strengthened to reduce the energy loss, the energy saving effect of VMD-MVR considerably increased.

Exergy performance of VMD-MVR was analyzed according to the experimental data acquired for the actual operation process (Table 6). The exergy input and exergy output were determined to be 4.95 and 0.259 kW, respectively. Consequently, the exergy efficiency was calculated to be 5.24%. Clearly, a large irreversible energy loss was still noticed in VMD-MVR. Accordingly, determining the parts with large exergy destruction was beneficial to improve the exergy performance of entire VMD-MVR. The exergy efficiency could only reflect the status of energy utilization during the entire thermal process rather than indicating the exergy distribution of various components in VMD-MVR. Therefore, it was necessary to analyze the energy utilization of each part within VMD-MVR, determine the main link of exergy destruction, and specify the direction for the further optimization design of VMD-MVR Fig. 8. depicts the exergy destruction distribution of each component, the total exergy destruction was found to be 4.691 kW, of which the exergy destruction of the compressor was as high as 1.580 kW, accounting for 33.68% of the total exergy destruction. Furthermore, the exergy destruction for the feed pump, heat exchanger, and VMD module were 1.03, 0.895, and 0.530 kW, accounting for 21.96, 19.08, and 11.3% of the total exergy destruction, respectively. Moreover, the exergy destruction caused by the high-temperature fluid flowing through pipes, valves, and other parts of VMD-MVR could not be ignored, accounting for nearly 13.98% of the total exergy destruction. Based on the abovementioned analysis, it is concluded that by improving the working performance of the critical components, such as

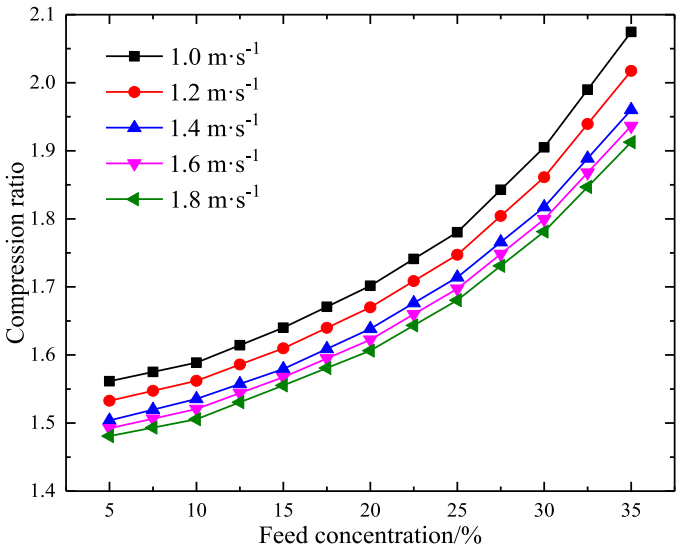

Fig. 18. Effect of feed velocity and feed concentration on compression ratio.

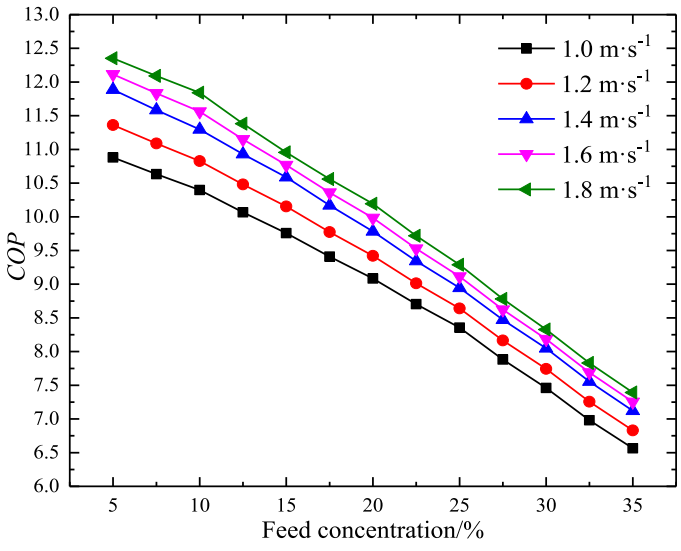

Fig. 20. Effect of feed velocity and feed concentration on *COP*.

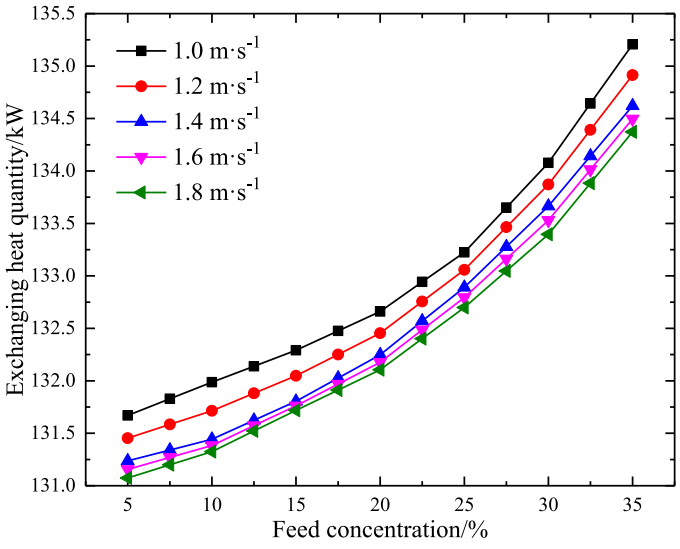

Fig. 19. Effect of feed velocity and feed concentration on exchanging heat quantity.

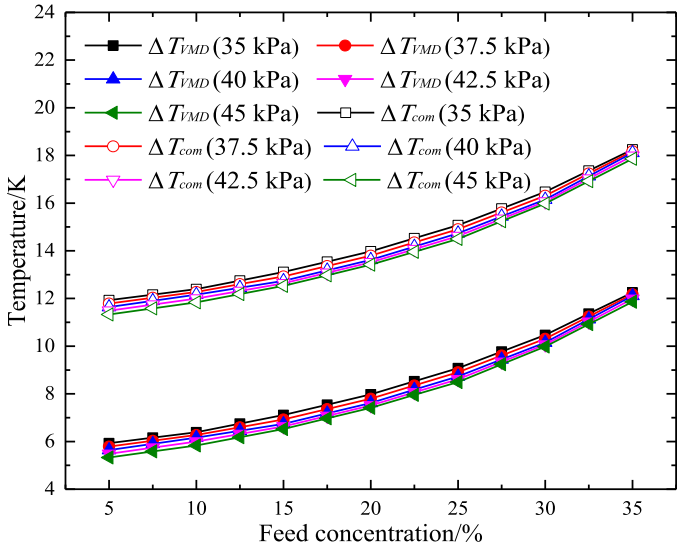

Fig. 21. Effect of permeate side pressure and feed concentration on ΔT_{VMD} and ΔT_{com}.

the heat exchanger, compressor, VMD module and feed pump, shortening the pipe length, and strengthening the insulation measures, the internal irreversibility degree and exergy destruction can be reduced, which would be the main direction for the optimization and improvement of VMD-MVR.

4.2. Simulation of the coupling of VMD with MVR

The simulation results of VMD-MVR proposed herein are presented and discussed in this section. Numerical simulation was executed using the developed mathematical models to examine the effects of several critical parameters on compression, condensation heat transfer, and exergy destruction of VMD-MVR, and the detailed design parameters for simulation are provided in Table 7.

4.2.1. Effects of critical parameters on compression and condensation heat transfer

Figs. 9–12 show the effects of feed concentration on ΔT_{VMD} and ΔT_{com}, compression ratio, exchanging heat quantity, and *COP*, respectively, under the following conditions: feed temperature: 358.0 K, feed velocity: 1.0 m·s^{-1}, and ΔT_{hex}: 6 K. In fact, a higher feed concentration would result in a higher viscosity of solution in the VMD module, which would increase the boundary layer thickness and the heat and mass transfer resistance during VMD. To ensure stable evaporation with a constant membrane flux, the permeate side pressure should be further reduced to provide the sufficient transmembrane driving pressure difference. Therefore, it is concluded that with an increase in the feed concentration, the corresponding ΔT_{VMD} and ΔT_{com} would also be substantially increased. Consequently, the compression ratio and power consumption during compression significantly enhanced, increasing the exchanging heat quantity in the heat exchanger. Accordingly, a reduction in the *COP* from 10.88 to 6.56 was observed with an increase in feed concentration from 5 to 35%.

Figs. 13–16 depict the effects of feed temperature on ΔT_{VMD} and ΔT_{com}, compression ratio, exchanging heat quantity, and *COP*, respectively, at different feed concentrations under the following conditions: feed velocity: 1.0 m·s^{-1} and ΔT_{hex}: 6 K. It was inferred that a higher feed temperature led to a higher activity of the water molecules in the

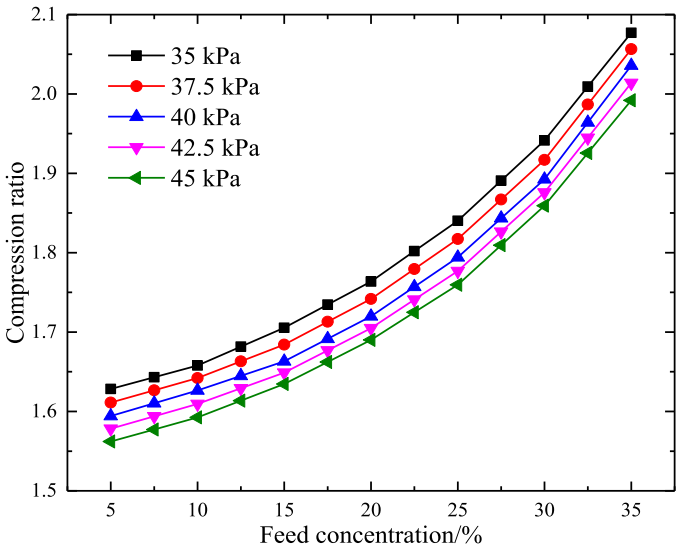

Fig. 22. Effect of permeate side pressure and feed concentration on compression ratio.

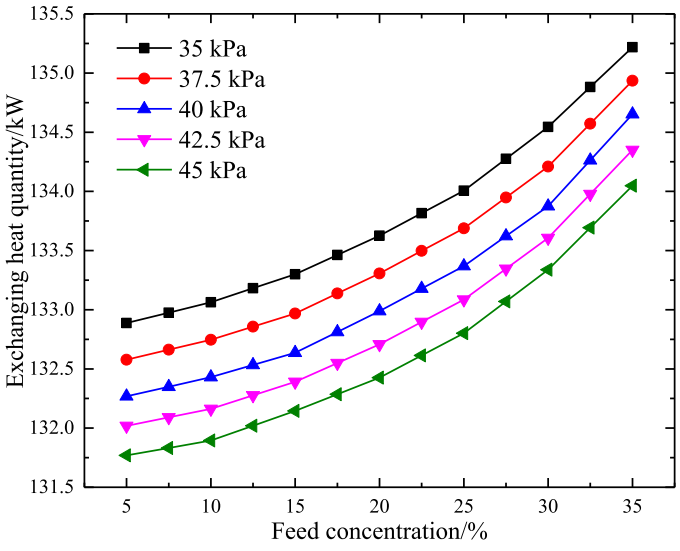

Fig. 23. Effect of permeate side pressure and feed concentration on exchanging heat quantity.

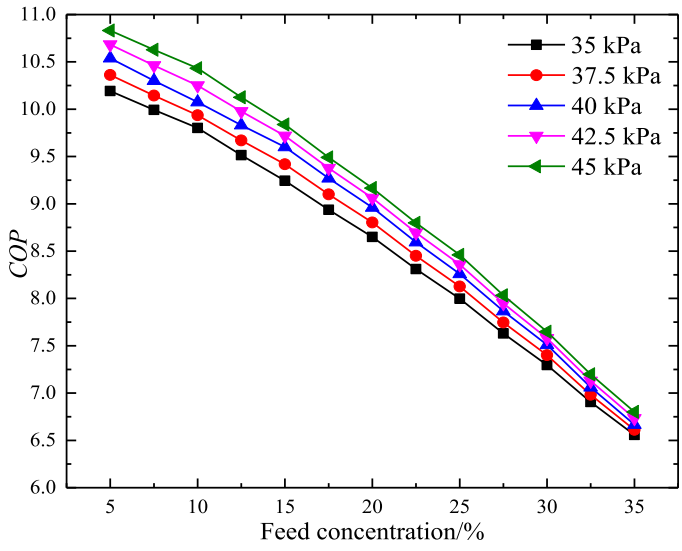

Fig. 24. Effect of permeate side pressure and feed concentration on *COP*.

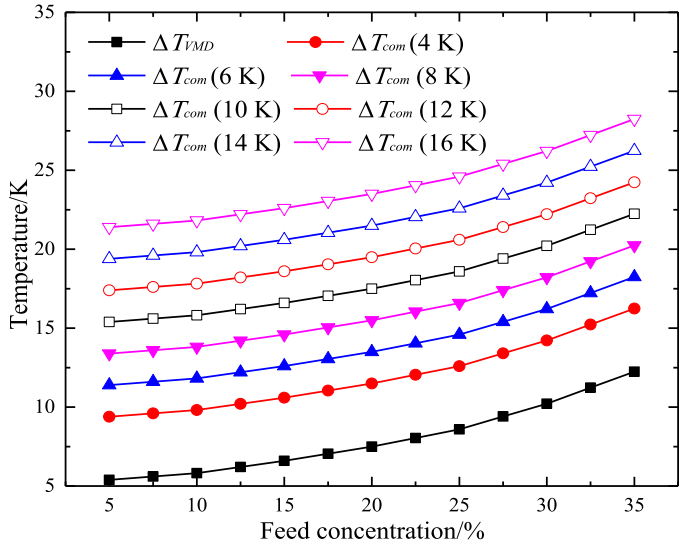

Fig. 25. Effect of ΔT_{hex} and feed concentration on ΔT_{VMD} and ΔT_{com}.

sulfuric acid solution, which accelerated the heat and mass transfer during VMD. Thus, the water molecules more easily evaporated because of the presence of sufficient heat at the membrane surface, and higher permeate side pressure was needed to maintain a constant membrane flux, which was beneficial for reducing both ΔT_{VMD} and ΔT_{com}. Consequently, with a decrease in the compression ratio and power consumption, the exchanging heat quantity decreased, whereas the *COP* increased. Taking the case of 20% feed concentration as an example, a 10.81% enhancement in the *COP* was attained (that is, from 8.60 to 9.53) with an increase in feed temperature from 353.0 to 363.0 K.

Figs. 17–20 show the effects of feed velocity on ΔT_{VMD} and ΔT_{com}, compression ratio, exchanging heat quantity, and *COP*, respectively, at different feed concentrations under the following conditions: feed temperature: 358.0 K and ΔT_{hex}: 6 K. Actually, with an increase in feed velocity, the stronger turbulence of solution and the thinner boundary layer in the VMD module contributed to the improvement of heat and mass transfer during VMD. Consequently, a higher permeate side pressure was needed to realize constant evaporation, and ΔT_{VMD} and ΔT_{com} accordingly decreased, which indicated that lower compression ratio and exchanging heat quantity were significantly required. As a result, the *COP* continuously increased with an increase in feed velocity. Taking the case of 10% feed concentration as an example, with an increase in feed velocity from 1.0 to 1.8 m·s^{-1}, a 13.46% enhancement was noticed in the *COP* (namely, from 10.4 to 11.8).

In previous studies, the effects of feed concentration, feed temperature, and feed velocity on compression and condensation heat transfer have been investigated by adjusting the permeate side pressure to maintain a constant evaporation rate in the VMD module. However, in this study, to examine the effect of the permeate side pressure on these two processes, the feed temperature was adjusted to maintain a constant evaporation in the VMD module Figs. 21–24. depict the effects of permeate side pressure on ΔT_{VMD} and ΔT_{com}, compression ratio, exchanging heat quantity, and *COP*, respectively, at different feed concentrations under the following conditions: feed velocity: 1.0 m·s^{-1} and ΔT_{hex}: 6 K. At a fixed feed concentration, the *COP* continuously increased with an increase in the permeate side pressure. In fact, a higher permeate side pressure led to a higher feed temperature, which reduced ΔT_{VMD} and ΔT_{com}. Accordingly, the corresponding compression ratio and power consumption continuously declined, which decreased

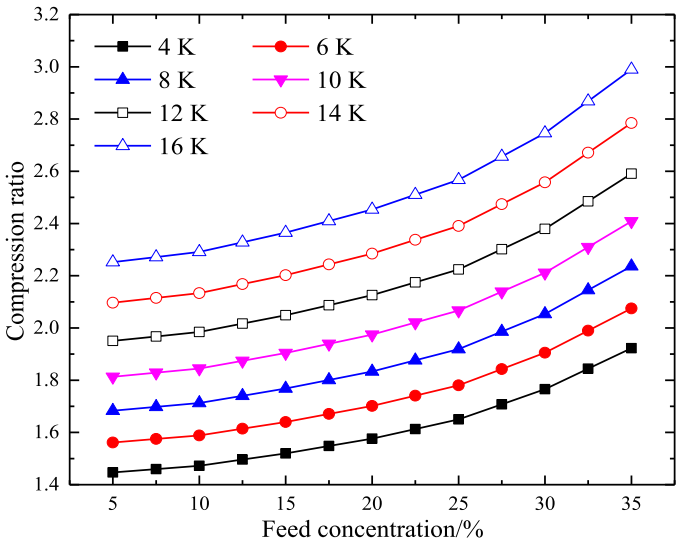

Fig. 26. Effect of ΔT_{hex} and feed concentration on compression ratio.

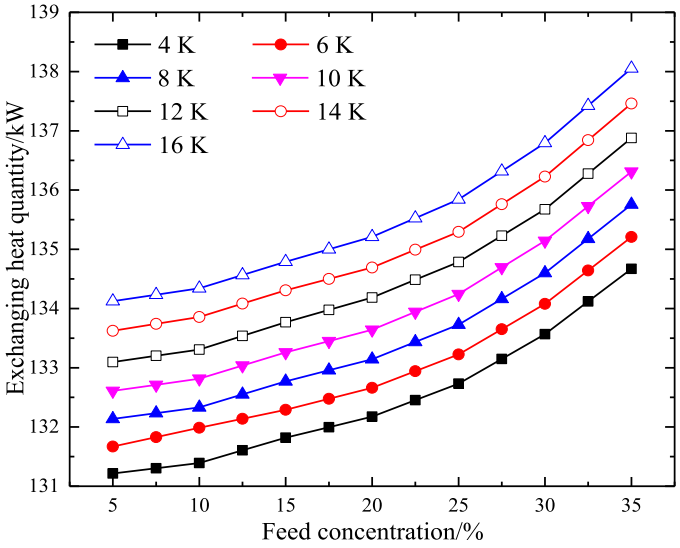

Fig. 27. Effect of ΔT_{hex} and feed concentration on exchanging heat quantity.

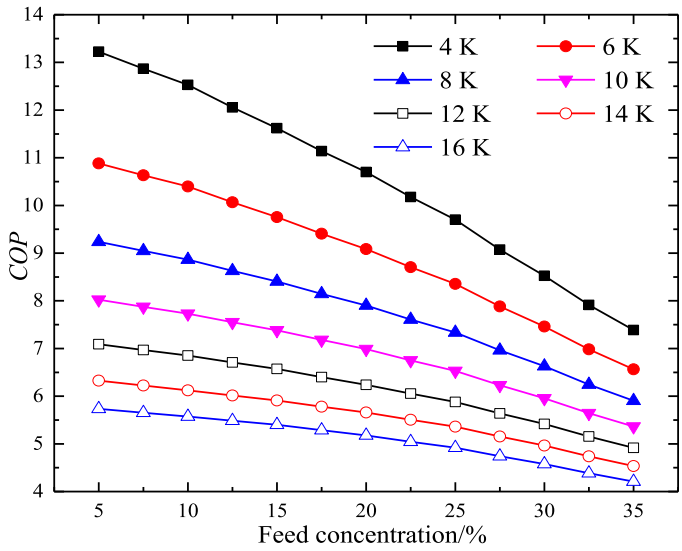

Fig. 28. Effect of ΔT_{hex} and feed concentration on *COP*.

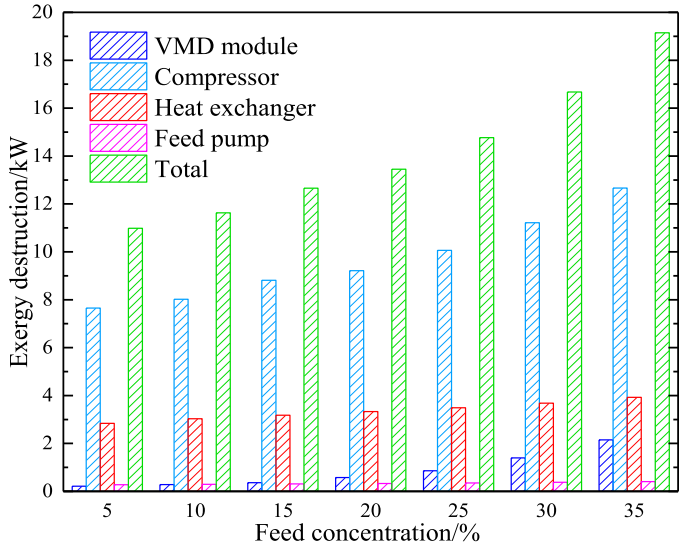

Fig. 29. Effect of feed concentration on exergy destruction in VMD-MVR.

the exchanging heat quantity. Consequently, the *COP* increased with the elevation of the permeate side pressure. Taking the case of 5% feed concentration as an example, with the elevation of the permeate side pressure from 35 to 45 kPa, a 6.28% enhancement was noticed in the *COP* (that is, from 10.19 to 10.83).

Figs. 25–28 depict the effects of ΔT_{hex} on ΔT_{VMD} and ΔT_{com}, compression ratio, exchanging heat quantity, and *COP*, respectively, at different feed concentrations under the following conditions: feed temperature: 358.0 K and feed velocity: 1.0 m·s^{-1}. At a fixed feed concentration, with an increase in the ΔT_{hex}, the *COP* decreased. In fact, with an increase in ΔT_{hex}, ΔT_{com} continuously increased, whereas ΔT_{VMD} demonstrated a very slight fluctuation, which could be neglected, and the compression ratio and power consumption accordingly increased. As a result, the exchanging heat quantity also constantly increased, which reduced the *COP*. Taking the case of 30% feed concentration as an example, with an increase in ΔT_{hex} from 4 to 16 K, a 46.31% decline was observed in the *COP* (that is, from 8.53 to 4.58).

4.2.2. *Effects of critical parameters on exergy destruction*

Herein, via simulation, the effects of critical parameters on exergy destruction in VMD-MVR were determined for the sulfuric acid solution treatment Fig. 29. shows the effects of feed concentration on exergy destruction in VMD-MVR under the following conditions: feed temperature: 358.0 K, feed velocity: 1.0 m·s^{-1}, and ΔT_{hex}: 6 K. In the VMD module, with an increase in feed concentration, the heat and mass transfer resistance during VMD increased, increasing the irreversibility degree; therefore, the exergy destruction in the VMD module accordingly increased. For the compressor, a higher power was required with an increase in feed concentration, which increased the temperature difference between inlet and outlet and the irreversibility degree during compression. Consequently, the exergy destruction in compressor increased. In the case of heat exchanger, the temperature difference between the heat exchange fluids increased with an increase in feed concentration, and the irreversibility degree during heat exchange also increased, which increased the exergy destruction in heat exchanger. For the feed pump, with an increase in feed concentration, the irreversibility degree increased owing to the increase in power consumption caused by the higher flow rate of the solution, increasing the exergy destruction in the feed pump. Therefore, the total exergy destruction in VMD-MVR increased with an increase in feed concentration.

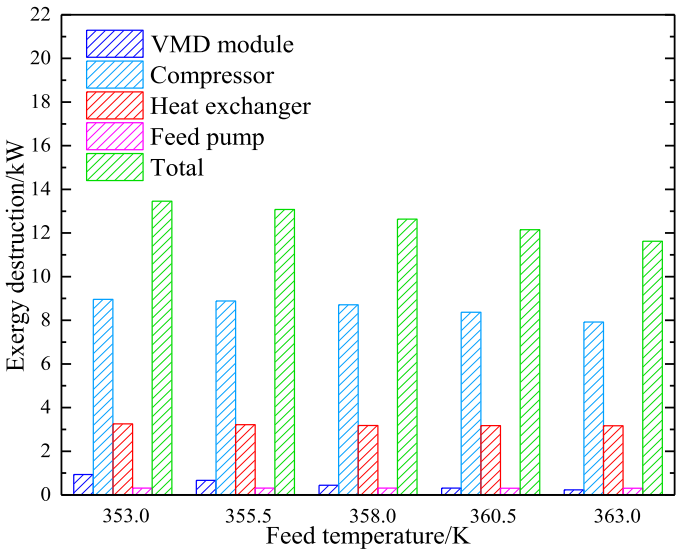

Fig. 30. Effect of feed temperature on exergy destruction in VMD-MVR.

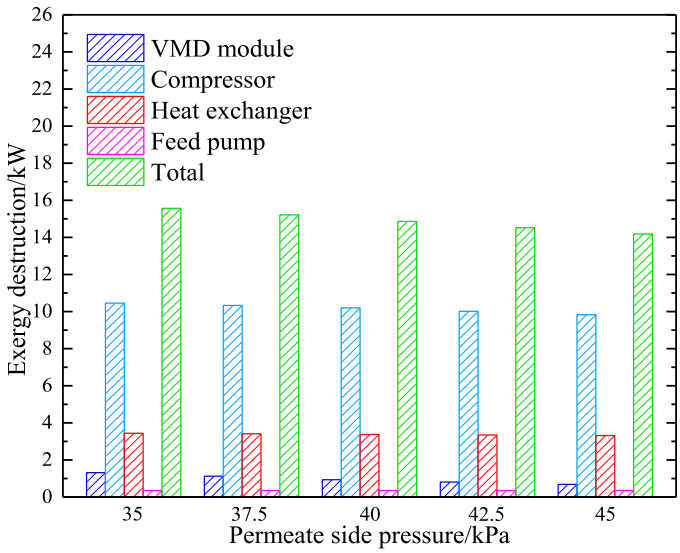

Fig. 32. Effect of permeate side pressure on exergy destruction in VMD-MVR.

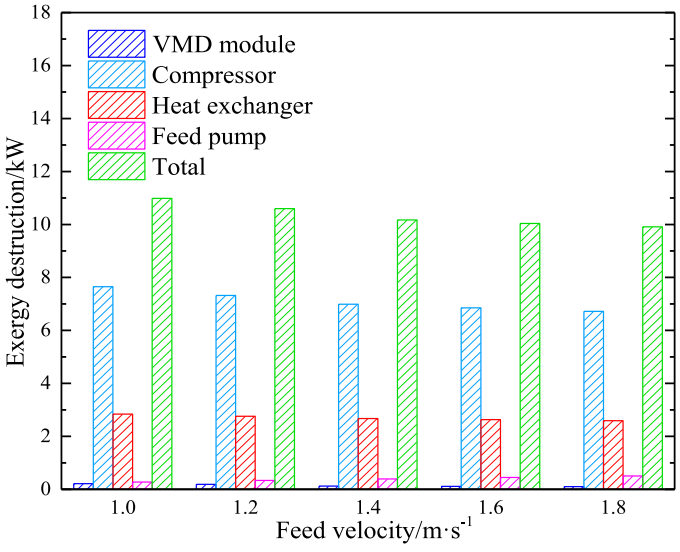

Fig. 31. Effect of feed velocity on exergy destruction in VMD-MVR.

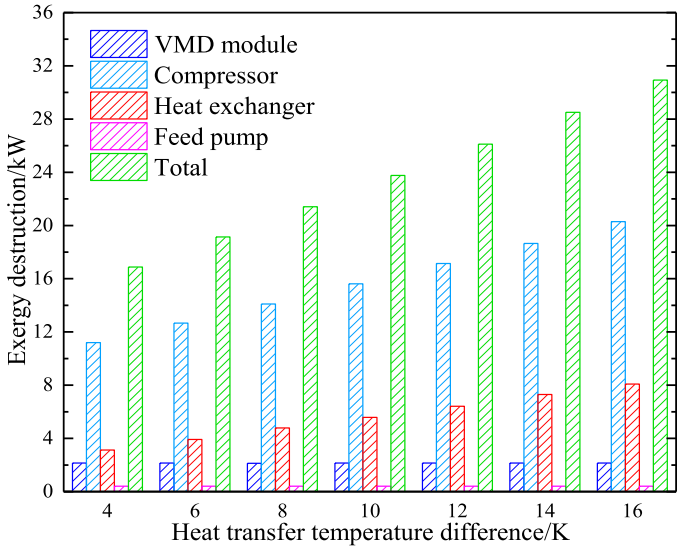

Fig. 33. Effect of ΔT_{hex} on exergy destruction in VMD-MVR.

Fig. 30 shows the effect of feed temperature on exergy destruction in VMD-MVR under the following conditions: feed concentration: 15%, feed velocity: 1.0 m·s^{-1}, and ΔT_{hex}: 6 K. In the VMD module, with an increase in feed temperature, the irreversibility degree reduced due to the decrease in the mass and heat transfer resistance, decreasing the exergy destruction in the VMD module. For the compressor, an increase in feed temperature directly decreased the power and temperature difference between the inlet and the outlet, and the irreversibility degree during compression reduced; thus, the exergy destruction in the compressor decreased. In the case of the heat exchanger, an increase in feed temperature decreased the temperature difference between the heat exchange fluids in the heat exchanger and decreased the irreversibility degree during heat exchange, which decreased the exergy destruction in the heat exchanger. For the feed pump, a higher feed temperature resulted in a lower power consumption and irreversibility degree, which correspondingly reduced the exergy destruction in the feed pump. Consequently, it was inferred that with the elevation of feed temperature, the total exergy destruction in VMD-MVR decreased.

Fig. 31 depicts the effect of feed velocity on exergy destruction in VMD-MVR under the following conditions: feed concentration: 5%, feed temperature: 358.0 K, and ΔT_{hex}: 6 K. In the VMD module, the increase in feed velocity decreased the irreversibility degree because of the decrease in the mass and heat transfer resistance, which decreased the exergy destruction. For the compressor, a higher feed velocity led to a lower power consumption, decreasing the temperature difference between the inlet and the outlet and the irreversibility degree during compression, which accordingly reduced the exergy destruction in the compressor. In the case of the heat exchanger, an increase in feed velocity decreased the temperature difference between the heat exchange fluids and the irreversibility degree during heat exchange, decreasing the exergy destruction in the heat exchanger. For the feed pump, as feed velocity increased, the power consumption and the irreversibility degree increased, which increased the exergy destruction. Thus, the total exergy destruction substantially decreased despite a slight increase in exergy destruction in the feed pump.

Fig. 32 shows the effect of permeate side pressure on exergy destruction in VMD-MVR under the following conditions: feed concentration: 25%, feed velocity: 1.0 m·s^{-1}, and ΔT_{hex}: 6 K. In the VMD module, with an increase in the permeate side pressure, a higher feed temperature was required to maintain stable evaporation, and hence,

the irreversibility degree during VMD weakened. Accordingly, the exergy destruction in the VMD module gradually reduced. For the compressor, with an increase in permeate side pressure, the power consumption reduced, decreasing the irreversibility degree during compression. Consequently, the exergy destruction in the compressor decreased. In the case of the heat exchanger, with an increase in the permeate side pressure, the irreversibility degree decreased because of the lower temperature difference between the heat exchange fluids, which reduced the exergy destruction in the heat exchanger. For the feed pump, with an increase in the permeate side pressure, the power consumption and irreversibility degree decreased, which decreased the exergy destruction in the feed pump. Clearly, the total exergy destruction in VMD-MVR reduced with an increase in the permeate side pressure.

Fig. 33 depicts the effect of ΔT_{hex} on exergy destruction in VMD-MVR under the following conditions: feed concentration: 35%, feed temperature: 358.0 K, and feed velocity: 1.0 $m{\cdot}s^{-1}$. In the VMD module and feed pump, the increase in ΔT_{hex} did not directly affect the exergy destruction. For the compressor, with an increase in the ΔT_{hex}, the power consumption and the irreversibility degree increased, which increased the exergy destruction in the compressor. In the case of the heat exchanger, the increase in ΔT_{hex} directly increased the irreversibility degree; accordingly, the exergy destruction in the heat exchanger increased. Thus, the total exergy destruction in VMD-MVR increased with an increase in the ΔT_{hex}.

5. Conclusions

This study focused on dealing with the sulfuric acid waste by a VMD system based on MVR. Employing the established mathematical models, the energy and exergy analysis was conducted based on the actual operation data. Furthermore, the effects of important parameters on compression and condensation heat transfer of secondary vapors were analyzed using the Matlab software. Finally, the effects of critical parameters on exergy destruction in VMD-MVR were also simulated and investigated. The significant findings achieved after detailed investigation were provided as follows:

(1) Membrane flux, separation efficiency, ΔT_{VMD}, ΔT_{com}, *SHEC*, and *COP* were 1.7 $kg{\cdot}m^{-2}{\cdot}h^{-1}$, 99.9%, 1.3 K, 3.3 K, 80.88 $kWh{\cdot}t^{-1}$, and 7.88, respectively, under the following conditions: feed concentration: 5%; feed temperature: 353.0 K; feed velocity: 1.6 $m{\cdot}s^{-1}$; permeate side pressure: 45 kPa; ΔT_{hex}: 2 K; and compressor frequency: 40 Hz. Furthermore, via the exergy analysis, the exergy input, exergy destruction, exergy output, and exergy efficiency were determined to be 4.95 kW, 4.691 kW, 0.259 kW, and 5.24%, respectively.

(2) According to the parametric analysis based on the simulations, it was concluded that with a decrease in feed concentration or increase in feed temperature, feed velocity, and permeate side pressure, ΔT_{VMD}, ΔT_{com}, compression ratio, and exchanging heat quantity decreased, which increased the *COP*. However, with an increase in the ΔT_{hex}, ΔT_{com} increased, increasing the compression ratio and exchanging heat quantity and decreasing the *COP*. In addition, decreasing the feed concentration and ΔT_{hex} or increasing the feed temperature, feed velocity, and permeate side pressure, decreased the total exergy destruction in VMD-MVR system.

The abovementioned results indicate that the application of VMD-MVR in the sulfuric acid waste treatment for reducing energy consumption and improving separation efficiency is an interesting approach. The present study mainly focused on the evaporation characteristics of VMD-MVR using a low-concentration sulfuric acid solution. Consequently, more experiments will be performed in the future using a high-concentration sulfuric acid solution, which will provide significant theoretical guidance and technical support for the design and optimization of VMD-MVR.

CRediT authorship contribution statement

Zetian Si: Methodology, Investigation, Writing – original draft. **Dong Han:** Formal analysis. **Yulei Xing:** Validation, Data curation. **Jiawei Xiang:** Supervision, Project administration, Investigation, Resources, Writing – review & editing.

Declaration of Competing Interest

The authors declare that they have no known competing financial interests or personal relationships that could have appeared to influence the work reported in this paper.

Acknowledgements

The authors acknowledge the financial support from the National Natural Science Foundation of China (No. U1909217), the Zhejiang Natural Science Foundation of China (No. LD21E050001), the Zhejiang Special Support Program for High-level Personnel Recruitment of China (No. 2018R52034), the Wenzhou Major Science and Technology Innovation Project of China (No. ZG2020051), and Tianjin Technical Cooperation R&D and Industrialization Projects for the Belt and Road Initiative (18YDYGHZ00100) .

Supplementary materials

Supplementary material associated with this article can be found, in the online version, at doi:10.1016/j.cep.2022.108862.

References

[1] L. Huaqing, X. Jianzhong, C. Kangjie, M. Junquan, et al., Fabrication of high-performance pervaporation membrane for sulfuric acid recovery via interfacial polymerization, J. Membr. Sci. 624 (2021), 119108, https://doi.org/10.1016/J.MEMSCI.2021.119108.
[2] G. Hui, Y. Pengyi, P. Vladimir, et al., Ammonium sulfate production from wastewater and low-grade sulfuric acid using bipolar- and cation-exchange membranes, J. Clean. Prod. 285 (2021), 124888, https://doi.org/10.1016/J.JCLEPRO.2020.124888.
[3] Y. Du, Y. Wen, H. Fan, Elimination of Cr(VI) from chromium slag with poplar lignin by electrochemical treatment in sulfuric acid solution, Environ. Sci. Pollut. R. 27 (2020) 29441–29450, https://doi.org/10.1007/s11356-020-09289-9.
[4] A.A. H, S. Sergio, P. Antonio, Photothermal sweeping gas membrane distillation and reverse electrodialysis for light-to-heat-to-power conversion, Chem. Eng. Process. 164 (2021), 108382, https://doi.org/10.1016/J.CEP.2021.108382.
[5] G. Viader, O. Casal, B. Lefèvre, N. de Arespacochaga, et al., Integration of membrane distillation as volume reduction technology for in-land desalination brines management: pre-treatments and scaling limitations, J. Environ. Manage. 289 (2021), 112549, https://doi.org/10.1016/J.JENVMAN.2021.112549.
[6] V. Karanikola, SE. Moore, A. Deshmukh, Economic performance of membrane distillation configurations in optimal solar thermal desalination systems, Desalination 472 (2019), 114164, https://doi.org/10.1016/j.desal.2019.114164.
[7] M.M.A. Shirazi, A. Kargari, M. Tabatabaei, Evaluation of commercial PTFE membranes in desalination by direct contact membrane distillation, Chem. Eng. Process. 76 (2014) 16–25, https://doi.org/10.1016/j.cep.2013.11.010.
[8] U.K. Kesieme, N. Milne, C.Y. Cheng, Recovery of water and acid from leach solutions using direct contact membrane distillation, Water. Sci. Technol. 69 (2013) 868–875, https://doi.org/10.2166/wst.2013.788.
[9] X. Li, Y. Qin, R. Liu, Study on concentration of aqueous sulfuric acid solution by multiple-effect membrane distillation, Desalination 307 (2012) 34–41, https://doi.org/10.1016/j.desal.2012.08.023.
[10] G. Zhang, Q. Zhang, K. Zhou, Study on concentrating sulfuric acid solution by vacuum membrane distillation, J. Cent. South Univ. Technol. 6 (1999) 99–102, https://doi.org/10.1007/s11771-999-0007-5.
[11] H. Dahmardeh, H.A. Akhlaghi Amiri, S.M. Nowee, Evaluation of mechanical vapor recompression crystallization process for treatment of high salinity wastewater, Chem. Eng. Process. 145 (2019), 107682, https://doi.org/10.1016/j.cep.2019.107682.
[12] Y. Kansha, A. Kishimoto, A. Tsutsumi, Application of the self-heat recuperation technology to crude oil distillation, Appl. Therm. Eng. 43 (2012) 153–157, https://doi.org/10.1016/j.applthermaleng.2011.10.022.
[13] S. Ai, B. Wang, X. Li, W. Shi, Numerical analysis on the performance of mechanical vapor recompression system for strong sodium chloride solution enrichment, Appl.

Therm. Eng. 137 (2018) 386–394, https://doi.org/10.1016/j.applthermaleng.2018.03.104.
[14] L. Liang, D. Han, R. Ma, Treatment of high-concentration wastewater using double-effect mechanical vapor recompression, Desalination 314 (2013) 139–146, https://doi.org/10.1016/j.desal.2013.01.016.
[15] E. Ayati, Z. Rahimi-Ahar, M.S. Hatamipour, Performance evaluation of a heat pump-driven vacuum humidification-dehumidification desalination system, Appl. Therm. Eng. 180 (2020), 115872, https://doi.org/10.1016/j.applthermaleng.2020.115872.
[16] Z.Y. Xu, J.T. Gao, H.C. Mao, Double-section absorption heat pump for the deep recovery of low-grade waste heat, Energ. Convers. Manage. 220 (2020), 113072, https://doi.org/10.1016/j.enconman.2020.113072.
[17] W.F. He, D. Han, C. Ji, Investigation on humidification dehumidification desalination system coupled with heat pump, Desalination 436 (2018) 152–160, https://doi.org/10.1016/j.desal.2018.02.021.
[18] L. Shaowu, Q. Yan, L. Dong, Handbook of Sulfuric Acid, Southeast University Press, Nanjing, 2001 (In Chinese).
[19] M.R. Qtaishat, F. Banat, Desalination by solar powered membrane distillation systems, Desalination 308 (2013) 186–197, https://doi.org/10.16606/j.desal.2012.01.021.
[20] Y.D. Kim, K. Thu, S.H. Choi, Solar-assisted multi-stage vacuum membrane distillation system with heat recovery unit, Desalination 367 (2015) 161–171, https://doi.org/10.1016/j.desal.2015.04.003.
[21] C.K. Chiam, R. Sarbatly, Heat transfer in the rectangular cross-flow flat-sheet membrane module for vacuum membrane distillation, Chem. Eng. Process. 79 (2014) 23–33, https://doi.org/10.1016/j.cep.2014.03.005.
[22] R.H. liu, D. Chen, Y.L. Peng, Mathematical modeling and optimal operation condition analysis of heat pump two-effect direct contact membrane distillation system, Mater. Sci. Eng. 612 (2019), 032004, https://doi.org/10.1088/1757-899X/612/3/032004.
[23] W.K. Pang, W.J. Ling, Q.L. Pan, Performance analysis of mechanical vapor recompression heat pump driven by centrifuge fan, J. Mech. Eng. 49 (2013) 142–146, https://doi.org/10.3901/JME.2013.12.142 (In Chinese).
[24] W.F. He, J.J. Chen, M.R. Zhen, D. Han, Thermodynamic, economic analysis and optimization of a heat pump driven desalination system with open-air humidification dehumidification configurations, Energy 174 (2019) 768–778, https://doi.org/10.1016/j.energy.2019.03.005.
[25] R. Miladi, N. Frikha, S. Gabsi, Exergy analysis of a solar-powered vacuum membrane distillation unit using two models, Energy 120 (2017) 872–883, https://doi.org/10.1016/j.energy.2016.11.133.
[26] N. Diban, O.C. Voinea, A. Urtiaga, I. Ortiz, Vacuum membrane distillation of the main pear aroma compound: experimental study and mass transfer modeling, J. Membr. Sci. 326 (2009) 64–75, https://doi.org/10.1016/j.memsci.2008.09.024.
[27] K. Chen, C. Xiao, Q. Huang, Study on vacuum membrane distillation (VMD) using FEP hollow fiber membrane, Desalination 375 (2015) 24–32, https://doi.org/10.1016/j.desal.2015.07.021.
[28] Y. Zhou, C. Shi, G. Dong, Analysis of a mechanical vapor recompression wastewater distillation system, Desalination 353 (2014) 91–97, https://doi.org/10.1016/j.desal.2014.09.013.